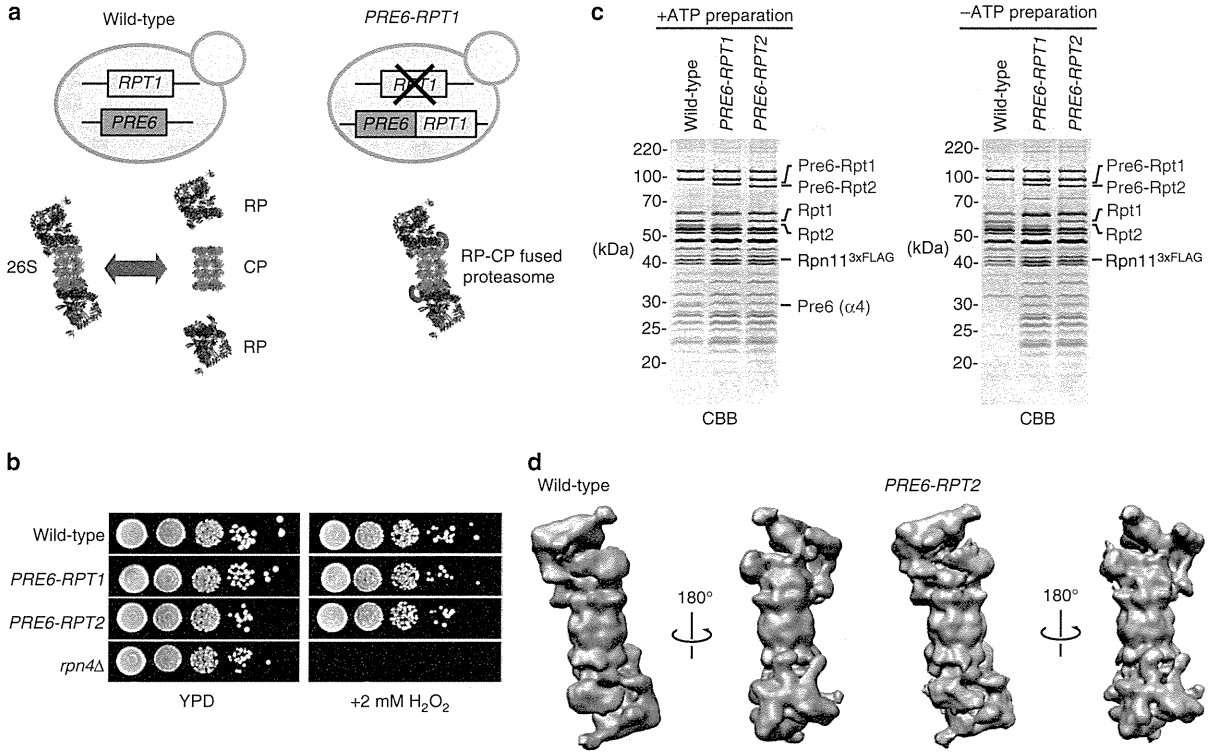

Figure 6 | Construction of genetically stabilized proteasomes. (**a**) Construction of the RP-CP-fused proteasome strain. To stabilize the RP-CP interaction *in vivo*, cells expressing Pre6-Rpt1 or Pre6-Rpt2 fusion protein were generated. (**b**) The RP-CP-fused cells exhibited wild-type growth. Wild-type (W303-1A), Pre6-Rpt1-fused (YYS961), Pre6-Rpt2-fused (YYS972) and *rpn4Δ* (YAT1894) cells were spotted onto YPD plates containing 0 or 2 mM H_2O_2, and then incubated at 25 °C. (**c**) SDS-polyacrylamide gel electrophoresis (SDS-PAGE) analysis of RP-CP-fused proteasomes. Proteasomes from wild-type (YYS40), Pre6-Rpt1-fused (YYS961) or Pre6-Rpt2-fused (YYS972) cells were affinity-purified using the 3 × FLAG tag in the presence (left) or absence of ATP (right). The proteasomes were subjected to SDS-PAGE followed by coomassie brilliant blue (CBB) staining. Protein bands corresponding to Rpt1, Rpt2, Pre6, $Rpn11^{3\times FLAG}$, Pre6-Rpt1, Pre6-Rpt2, and CP subunits are indicated. A full scan of the gel is provided in Supplementary Fig. 8. (**d**) Three-dimensional structure of the RP-CP-fused proteasome. Two different views of the cryo-EM maps are represented. The resolution of the wild-type structure is 27 Å, and that of the RP-CP-fused structure is 25 Å.

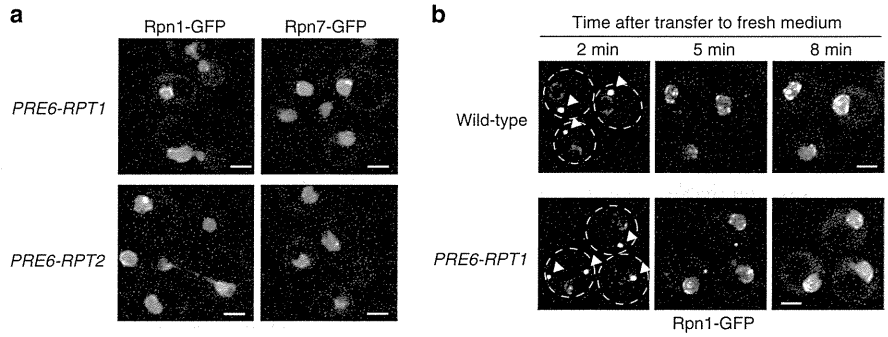

Figure 7 | Nuclear distribution of genetically stabilized proteasomes. (**a**) Subcellular distributions of RP-CP-fused proteasomes. Wild-type and RP-CP-fused cells expressing Rpn1-GFP or Rpn7-GFP (YYS1437, YYS1438, YYS1457, YYS1459, YYS1497 and YYS1498) were imaged by confocal microscopy. Scale bars, 2 μm. (**b**) Assay for nuclear re-import of proteasomes. Wild-type or *PRE6-RPT1* cells expressing Rpn1-GFP (YYS2117 and YYS2119) were cultured for 2 days to form PSGs. Immediately after transfer to fresh medium, the cells were mounted on glass slides and imaged by confocal microscopy at the indicated time points. PSGs are indicated by arrowheads. Scale bars, 2 μm.

assembled into the 26S proteasome[19–21]. In contrast to this canonical pathway, our results obtained by FCS/FCCS analysis of the importin mutant and cells expressing genetically stabilized proteasomes (Fig. 5; Supplementary Fig. 7) suggest that the 26S proteasome is assembled in the cytoplasm. Because we could not detect proteasome intermediates by FCS, even in the importin mutant, we cannot rule out the possibility of the canonical pathway. Clearly, further studies are needed to clarify which pathway predominates within cells. Regardless, our results strongly suggest that the nuclear import of the precursors is not

essential for proteasome assembly (Fig. 5; Supplementary Fig. 6). Furthermore, the results of nuclear import assays performed on RP-CP–fused proteasomes suggest that the 26S holoenzyme can translocate through the NPC (Fig. 7). Because the dimensions of the 26S proteasome are 20 nm × 45 nm, we speculate that the proteasome could be transported along its longitudinal axis through the 39-nm NPC channel[25]. The direction and orientation of translocation might be governed by Sts1, an NLS-containing protein that binds the lid subunit Rpn11 (ref. 22).

In summary, we have demonstrated a method for quantitative imaging analysis that enables direct observation of proteasome dynamics in living yeast cells in which all component proteins expressed at their endogenous levels. We unambiguously determined the local concentrations of the proteasome in distinct subcellular compartments, and also characterized the process of proteasome complex formation. Our live-cell paradigm avoids the potential artifacts of classical biochemical studies of the 26S proteasome, which is a labile complex *in vitro*. The 26S proteasome is an attractive target for pharmaceutical development[47], and the proteasome dynamics revealed by '*in vivo* biochemistry' provide a new perspective that should facilitate the development of next-generation proteasome inhibitors.

Methods

Yeast strains and media. Strains used in this study are listed in Supplementary Table 1. Standard protocols were used for yeast manipulation[48]. The proteasome subunits *RPN1*, *RPN7* and *PRE6* were chromosomally tagged with yeast enhanced green fluorescent protein (GFP) or monomeric Cherry fluorescent protein (mCherry), as described previously[21,40,49]. Genetically stabilized 26S proteasomes in which the CP subunit *PRE6*/α4 was fused to the RP subunit *RPT1* or *RPT2* were constructed as follows. The 5′-truncated *PRE6* open reading frame (ORF) (+304 to +762, *Not*I-*Bam*HI) was inserted into the *Not*I-*Bam*HI site of the yeast-integrating vector pRS306. Next, the *RPT1* ORF with its transcriptional terminator (+1 to +1,753, *Bam*HI-*Sal*I) or the *RPT2* ORF with its terminator (+1 to +1,633, *Bam*HI-*Xho*I) was inserted into the *Bam*HI-*Xho*I site of pRS306-5′*Δpre6*. The resulting plasmids, pOKA511, pRS306-5′*Δpre6-RPT1* and pOKA512, pRS306-5′*Δpre6-RPT2*, were linearized at the *Sal*I site within *PRE6* and transformed into *RPT1/rpt1Δ::LEU2* and *RPT2/rpt2Δ::HIS3*, respectively. Ura$^+$ transformants were sporulated, and tetrads were dissected. Because *RPT1* is an essential gene, Ura$^-$ Leu$^+$ spores did not germinate. However, we could obtain Ura$^+$ Leu$^+$ cells, indicating that the *PRE6-RPT1* fusion gene complements the *RPT1* deletion. Likewise, Ura$^-$ His$^+$ spores did not germinate, whereas Ura$^+$ His$^+$ cells could be obtained, indicating that the *PRE6-RPT2* fusion gene complements the *RPT2* deletion. To generate ρ^0 mutants, cells were cultured in YPD containing 10 μg ml^{-1} ethidium bromide for 24 h, and diluted cells were streaked onto YPD plates; the resultant colonies were then screened for inability to grow on YPGly plates[50].

Fluorescence correlation spectroscopy. Yeast cells chromosomally expressing GFP- and/or mCherry-tagged proteins were grown in SC medium (0.67% yeast nitrogen base without amino acids, 0.5% casamino acids, 2% glucose, 20 mg/l tryptophan, 20 mg/l uracil, 400 mg/l adenine, and 10 mM phosphate buffer, pH 7.5) at 25 °C to logarithmic phase, and then the cultures were shifted to 37 °C for the indicated times. The cells were mounted on a glass-bottom dish (MatTek Corporation). FCS and FCCS measurements were all performed at 25 °C with a ConfoCor2 (Carl Zeiss) microscope, as described[31,51–53]. The ConfoCor2 consisted of a CW Ar$^+$ and He–Ne lasers, a water-immersion objective (C-Apochromat, 40 ×, 1.2 numerical aperture; Carl Zeiss), and two channels of avalanche photodiodes (SPCM-200-PQ; EG&G). GFP was excited with the 488-nm laser line, and RFP with the 543-nm laser line, with the minimal total power that yielded a sufficient signal-to-noise ratio. The confocal pinhole diameter was adjusted to 70 μm for 488 nm and 78 μm for 543 nm. The emission signals were split by a dichroic mirror (570-nm beam splitter) and detected at 505–530 nm in the green channel (for GFP) and 600–650 nm in the red channel (for RFP). Simultaneous excitation of GFP- and mCherry/RFP-tagged proteins was carefully carried out at minimal and optimal excitation powers, chosen to obtain sufficiently high signal-to-noise ratios for analysis of diffusion times while preventing artifacts such as saturation, blinking and photobleaching that might affect the results of such analyses. Because cell and nuclear sizes differ significantly between yeast mother and daughter cells, our FCS and FCCS measurements were carried out on mother cells of similar size throughout the study. However, it should be noted that the FCS/FCCS results did not differ substantially between large mother cells and small daughter cells (data not shown).

Data were analysed using the ConfoCor2 software, as described in our previous study. Briefly, the fluorescence auto-correlation functions of the red and green channels, $G_r(\tau)$ and $G_g(\tau)$, and the fluorescence cross-correlation function, $G_c(\tau)$, were calculated from

$$G_x(\tau) = 1 + \frac{\langle \delta I_i(t) \cdot \delta I_j(t+\tau) \rangle}{\langle I_i(t) \rangle \langle I_j(t) \rangle} \quad (1)$$

where τ denotes the time delay; I_i the fluorescence intensity of the red channel (i = r) or green channel (i = g); and $G_r(\tau)$, $G_g(\tau)$, and $G_c(\tau)$ denote the red ($i = j = x$ = r) and green ($i = j = x$ = g) auto-correlation functions and the cross-correlation function (i = r, j = g, x = c), respectively. The acquired $G_x(\tau)$ values were fitted using a one-, two- or three-component model:

$$G_x(\tau) = 1 + \frac{1}{N} \sum_i F_i \left(1 + \frac{\tau}{\tau_i}\right)^{-1} \left(1 + \frac{\tau}{s^2 \tau_i}\right)^{-1/2} \quad (2)$$

where F_i and τ_i are the fraction and diffusion time of component I, respectively; N is the average number of fluorescent particles in the excitation-detection volume defined by the radius w_0 and the length $2z_0$; and s is the structure parameter representing the ratio $s = z_0/w_0$. The structure parameter was calibrated using Rhodamine-6G (Rh6G) standard solution at room temperature. The relationship between absolute concentration and calculated N was calibrated using a known concentration of Rh6G or recombinant mGFP solution. The effect of photobleaching on evaluation of concentration was determined according to a previous study[31]. Fluorescence correlation functions (FCFs) in live cells were measured sequentially 5–10 times with duration of 10 s to minimize the photobleaching effect, because gradual photobleaching by cellular depletion of GFP (RFP) affected diffusion analysis of FCFs obtained from measurements of longer duration (Supplementary Fig. 1).

The diffusion time of component i, τ_i, is related to the translational diffusion coefficient D of component i by

$$\tau_i = \frac{w_{xy}^2}{4D_i} \quad (3)$$

The diffusion of a spherical molecule is related to various physical parameters by the Stokes–Einstein equation as follows.

$$D_i = \frac{\kappa_B T}{6\pi\eta r_i} \quad (4)$$

where T is the absolute temperature, r_i is the hydrodynamic radius of the spherical molecule, η is the fluid-phase viscosity of the solvent, and κ_B is the Boltzmann constant. The diffusion coefficient of GFP-tagged proteins in a solution sample with 1 cP viscosity was evaluated using the known diffusion coefficients (apparent molecular weights) of the Rh6G standard and the recombinant mGFP solutions: respectively, 280 and 78 μm^2 s^{-1}. For live cells, the diffusion coefficient (apparent molecular weight) of GFP-tagged proteins was evaluated using GFP (or mCherry) expressed in yeast cells. Data containing severe photobleaching, possibly resulting from a high proportion of immobilized fluorophores, were excluded from the diffusion analysis. For FCCS analysis, the amplitude of the cross-correlation function was normalized to the amplitude of the auto-correlation function of mCherry to calculate the relative cross-correlation amplitude ($[G_c(0) - 1]/[G_r(0) - 1]$)[28,52,53]. Interaction amplitude was represented by the relative cross-correlation amplitude corresponding to the fraction of associated molecules (N_c/N_g). All measured FCFs were globally fitted, using the model described above, with the software installed on the ConfoCor 2 system. FCFs of Rh6G, GFP (RFP) and GFP/RFP-tagged molecules in solution were well fitted by a one-component model (i = 1) with or without a triplet term). In living cells, both FCS and FCCS analyses revealed that the mobilities of GFP/mCherry-tagged subunits were well fitted by a two-component model, because the results of analyses using two- and three-component models did not differ significantly. Thus, any third (or higher-order) components were either very weak or otherwise undetectable by these methods. To estimate the diffusion coefficients, FCFs in live cells were fitted by a two-component model (i = 2, D_{fast} and D_{slow}) with or without a triplet term. Intriguingly, in the two-component analysis, FCFs of GFP- or mCherry-tagged subunits frequently exhibited D_{fast} values with $D > 10$ μm^2 s^{-1}, much larger than the value calculated from D of Pre6-GFP in solution (Supplementary Fig. 1) and the apparent viscosity of a yeast cell[51]. This fast component with a large D value was barely detected for FCFs of cross-correlation functions, which exclude independent photochemical effects (such as blinking) from the two fluorescent molecules (Supplementary Fig. 4). Therefore, this fast component for GFP- or mCherry-tagged proteins may be an apparent diffusional term, caused by blinking of the probes, even though the time scale of the blinking was different from that reported in a previous study[54]. Such data were excluded from FCS analysis. The details of the simulations of molecular shapes of various proteins from analyses of FCFs were described in our previous studies[31,55,56].

Fluorescence microscopy. Cells grown in SC medium, described above, were mounted on glass slides and observed with a BX52 fluorescence microscope (Olympus) equipped with a UPlanApo 100 ×, 1.45 numerical aperture objective (Olympus), a confocal scanner unit CSU22 (Yokogawa) and an ORCA-ER CCD camera (Hamamatsu Photonics), as described previously[21]. Images were processed using the IPLab software (Scanalytics Inc). For proteasome nuclear import assays

(Fig. 7b), we acquired images at 0.5-μm intervals in the Z focal plane, and then generated maximal projections of Z stacks.

Purification of 26S proteasomes and cryo-electron microscopy. Intact 26S proteasomes from wild-type yeast and the RP-CP–fused strain were purified using the Rpn11-3 × FLAG tag[57]. The cells cultured in YPD medium were lysed with glass beads in lysis buffer, 50 mM Tris-HCl, pH 7.5, 100 mM NaCl, 10 mM $MgCl_2$, 4 mM ATP and 10% glycerol. After removal of the glass beads, extracts were cleared by centrifugation and incubated with anti-FLAG M2 agarose beads (Sigma) for 2 h at 4 °C. Beads were washed three times with the same buffer and the intact 26S proteasomes were eluted with 400 μg ml^{-1} 3XFLAG peptide (Sigma). For enrichment of the double-capped 26S proteasomes, the eluted samples were subjected to a 15–40% sucrose density gradient, subsequently fractionated, and analysed by SDS-polyacrylamide gel electrophoresis. The vitrified samples were imaged using a Tecnai F20 transmission electron microscope[7]. Using XMIPP[58], we computed 25-Å and 27-Å resolution maps (Fourier–Shell correlation, FSC = 0.5) for the wild-type and RP-CP–fused proteasomes from 43,000 and 15,000 single particles, respectively.

References

1. Baumeister, W., Walz, J., Zuhl, F. & Seemuller, E. The proteasome: paradigm of a self-compartmentalizing protease. *Cell* **92,** 367–380 (1998).
2. Glickman, M. H. & Ciechanover, A. The ubiquitin-proteasome proteolytic pathway: destruction for the sake of construction. *Physiol. Rev.* **82,** 373–428 (2002).
3. Finley, D. Recognition and processing of ubiquitin-protein conjugates by the proteasome. *Annu. Rev. Biochem.* **78,** 477–513 (2009).
4. Schwartz, A. L. & Ciechanover, A. Targeting proteins for destruction by the ubiquitin system: implications for human pathobiology. *Annu. Rev. Pharmacol. Toxicol.* **49,** 73–96 (2009).
5. Lander, G. C. *et al.* Complete subunit architecture of the proteasome regulatory particle. *Nature* **482,** 186–191 (2012).
6. Lasker, K. *et al.* Molecular architecture of the 26S proteasome holocomplex determined by an integrative approach. *Proc. Natl Acad. Sci. USA* **109,** 1380–1387 (2012).
7. Sakata, E. *et al.* Localization of the proteasomal ubiquitin receptors Rpn10 and Rpn13 by electron cryomicroscopy. *Proc. Natl Acad. Sci. USA* **109,** 1479–1484 (2012).
8. da Fonseca, P. C., He, J. & Morris, E. P. Molecular model of the human 26S proteasome. *Mol. Cell* **46,** 54–66 (2012).
9. Saeki, Y. & Tanaka, K. Assembly and function of the proteasome. *Methods Mol. Biol.* **832,** 315–337 (2012).
10. Murata, S., Yashiroda, H. & Tanaka, K. Molecular mechanisms of proteasome assembly. *Nat. Rev. Mol. Cell Biol.* **10,** 104–115 (2009).
11. Tomko, Jr R. J. & Hochstrasser, M. Order of the proteasomal ATPases and eukaryotic proteasome assembly. *Cell Biochem. Biophys.* **60,** 13–20 (2011).
12. Bedford, L., Paine, S., Sheppard, P. W., Mayer, R. J. & Roelofs, J. Assembly, structure, and function of the 26S proteasome. *Trends Cell. Biol.* **20,** 391–401 (2010).
13. Nederlof, P. M., Wang, H. R. & Baumeister, W. Nuclear localization signals of human and Thermoplasma proteasomal alpha subunits are functional in vitro. *Proc. Natl Acad. Sci. USA* **92,** 12060–12064 (1995).
14. Enenkel, C., Lehmann, A. & Kloetzel, P. M. Subcellular distribution of proteasomes implicates a major location of protein degradation in the nuclear envelope-ER network in yeast. *EMBO J.* **17,** 6144–6154 (1998).
15. Wilkinson, C. R. *et al.* Localization of the 26S proteasome during mitosis and meiosis in fission yeast. *EMBO J.* **17,** 6465–6476 (1998).
16. Amsterdam, A., Pitzer, F. & Baumeister, W. Changes in intracellular localization of proteasomes in immortalized ovarian granulosa cells during mitosis associated with a role in cell cycle control. *Proc. Natl Acad. Sci. USA* **90,** 99–103 (1993).
17. Tsuchiya, H., Arai, N., Tanaka, K. & Saeki, Y. Cytoplasmic proteasomes are not indispensable for cell growth in Saccharomyces cerevisiae. *Biochem. Biophys. Res. Commun.* **436,** 372–376 (2013).
18. Wang, H. R., Kania, M., Baumeister, W. & Nederlof, P. M. Import of human and Thermoplasma 20S proteasomes into nuclei of HeLa cells requires functional NLS sequences. *Eur. J. Cell Biol.* **73,** 105–113 (1997).
19. Wendler, P., Lehmann, A., Janek, K., Baumgart, S. & Enenkel, C. The bipartite nuclear localization sequence of Rpn2 is required for nuclear import of proteasomal base complexes via karyopherin alphabeta and proteasome functions. *J. Biol. Chem.* **279,** 37751–37762 (2004).
20. Lehmann, A., Janek, K., Braun, B., Kloetzel, P. M. & Enenkel, C. 20S proteasomes are imported as precursor complexes into the nucleus of yeast. *J. Mol. Biol.* **317,** 401–413 (2002).
21. Isono, E. *et al.* The assembly pathway of the 19S regulatory particle of the yeast 26S proteasome. *Mol. Biol. Cell* **18,** 569–580 (2007).
22. Chen, L. *et al.* Sts1 plays a key role in targeting proteasomes to the nucleus. *J. Biol. Chem.* **286,** 3104–3118 (2011).
23. Savulescu, A. F. *et al.* Nuclear import of an intact preassembled proteasome particle. *Mol. Biol. Cell* **22,** 880–891 (2011).
24. Reits, E. A., Benham, A. M., Plougastel, B., Neefjes, J. & Trowsdale, J. Dynamics of proteasome distribution in living cells. *EMBO J.* **16,** 6087–6094 (1997).
25. Pante, N. & Kann, M. Nuclear pore complex is able to transport macromolecules with diameters of about 39 nm. *Mol. Biol. Cell* **13,** 425–434 (2002).
26. Hoelz, A., Debler, E. W. & Blobel, G. The structure of the nuclear pore complex. *Annu. Rev. Biochem.* **80,** 613–643 (2011).
27. Slaughter, B. D. & Li, R. Toward quantitative "in vivo biochemistry" with fluorescence fluctuation spectroscopy. *Mol. Biol. Cell* **21,** 4306–4311 (2010).
28. Sako, Y. *et al.* Live cell single-molecule detection in systems biology. *Wiley Interdiscip. Rev. Syst. Biol. Med.* **4,** 183–192 (2012).
29. Petrasek, Z., Ries, J. & Schwille, P. Scanning FCS for the characterization of protein dynamics in live cells. *Methods Enzymol.* **472,** 317–343 (2010).
30. Slaughter, B. D., Schwartz, J. W. & Li, R. Mapping dynamic protein interactions in MAP kinase signaling using live-cell fluorescence fluctuation spectroscopy and imaging. *Proc. Natl Acad. Sci. USA* **104,** 20320–20325 (2007).
31. Pack, C., Saito, K., Tamura, M. & Kinjo, M. Microenvironment and effect of energy depletion in the nucleus analyzed by mobility of multiple oligomeric EGFPs. *Biophys. J.* **91,** 3921–3936 (2006).
32. Wendler, P. *et al.* Atypical AAA+ subunit packing creates an expanded cavity for disaggregation by the protein-remodeling factor Hsp104. *Cell* **131,** 1366–1377 (2007).
33. Verschoor, A., Warner, J. R., Srivastava, S., Grassucci, R. A. & Frank, J. Three-dimensional structure of the yeast ribosome. *Nucleic Acids Res.* **26,** 655–661 (1998).
34. Laporte, D., Salin, B., Daignan-Fornier, B. & Sagot, I. Reversible cytoplasmic localization of the proteasome in quiescent yeast cells. *J. Cell Biol.* **181,** 737–745 (2008).
35. Haarer, B., Aggeli, D., Viggiano, S., Burke, D. J. & Amberg, D. C. Novel interactions between actin and the proteasome revealed by complex haploinsufficiency. *PLoS Genet.* **7,** e1002288 (2011).
36. Geng, F., Wenzel, S. & Tansey, W. P. Ubiquitin and proteasomes in transcription. *Annu. Rev. Biochem.* **81,** 177–201 (2012).
37. Roelofs, J. *et al.* Chaperone-mediated pathway of proteasome regulatory particle assembly. *Nature* **459,** 861–865 (2009).
38. Funakoshi, M., Tomko, Jr R. J., Kobayashi, H. & Hochstrasser, M. Multiple assembly chaperones govern biogenesis of the proteasome regulatory particle base. *Cell* **137,** 887–899 (2009).
39. Park, S. *et al.* Hexameric assembly of the proteasomal ATPases is templated through their C termini. *Nature* **459,** 866–870 (2009).
40. Saeki, Y., Toh-e, A., Kudo, T., Kawamura, H. & Tanaka, K. Multiple proteasome-interacting proteins assist the assembly of the yeast 19S regulatory particle. *Cell* **137,** 900–913 (2009).
41. Mannhaupt, G., Schnall, R., Karpov, V., Vetter, I. & Feldmann, H. Rpn4p acts as a transcription factor by binding to PACE, a nonamer box found upstream of 26S proteasomal and other genes in yeast. *FEBS Lett.* **450,** 27–34 (1999).
42. Wang, X., Yen, J., Kaiser, P. & Huang, L. Regulation of the 26S proteasome complex during oxidative stress. *Sci. Signal.* **3,** ra88 (2010).
43. Gonzalez, F., Delahodde, A., Kodadek, T. & Johnston, S. A. Recruitment of a 19S proteasome subcomplex to an activated promoter. *Science* **296,** 548–550 (2002).
44. Lassot, I. *et al.* The proteasome regulates HIV-1 transcription by both proteolytic and nonproteolytic mechanisms. *Mol. Cell* **25,** 369–383 (2007).
45. Nakamura, M. *et al.* Spt6 levels are modulated by PAAF1 and proteasome to regulate the HIV-1 LTR. *Retrovirology* **9,** 13 (2012).
46. Geng, F. & Tansey, W. P. Similar temporal and spatial recruitment of native 19 and 20S proteasome subunits to transcriptionally active chromatin. *Proc. Natl Acad. Sci. USA* **109,** 6060–6065 (2012).
47. Mullard, A. Next-generation proteasome blockers promise safer cancer therapy. *Nat. Med.* **18,** 7 (2012).
48. Sherman, F. Getting started with yeast. *Methods Enzymol.* **194,** 3–21 (1991).
49. Fukunaga, K., Kudo, T., Toh-e, A., Tanaka, K. & Saeki, Y. Dissection of the assembly pathway of the proteasome lid in Saccharomyces cerevisiae. *Biochem. Biophys. Res. Commun.* **396,** 1048–1053 (2010).
50. Fox, T. D. *et al.* Analysis and manipulation of yeast mitochondrial genes. *Methods Enzymol.* **194,** 149–165 (1991).
51. Kawai-Noma, S. *et al.* Dynamics of yeast prion aggregates in single living cells. *Genes Cells* **11,** 1085–1096 (2006).
52. Park, H., Pack, C., Kinjo, M. & Kaang, B. K. *In vivo* quantitative analysis of PKA subunit interaction and cAMP level by dual color fluorescence cross correlation spectroscopy. *Mol. Cells* **26,** 87–92 (2008).

53. Noda, Y. *et al.* Reciprocal interaction with G-actin and tropomyosin is essential for aquaporin-2 trafficking. *J. Cell Biol.* **182,** 587–601 (2008).
54. Haupts, U., Maiti, S., Schwille, P. & Webb, W. W. Dynamics of fluorescence fluctuations in green fluorescent protein observed by fluorescence correlation spectroscopy. *Proc. Natl Acad. Sci. USA* **95,** 13573–13578 (1998).
55. Pack, C. G. *et al.* Analysis of interaction between chaperonin GroEL and its substrate using fluorescence correlation spectroscopy. *Cytometry* **36,** 247–253 (1999).
56. Kawai-Noma, S. *et al. In vivo* evidence for the fibrillar structures of Sup35 prions in yeast cells. *J. Cell Biol.* **190,** 223–231 (2010).
57. Saeki, Y., Isono, E. & Toh-e, A. Preparation of ubiquitinated substrates by the PY motif-insertion method for monitoring 26S proteasome activity. *Methods Enzymol.* **399,** 215–227 (2005).
58. Scheres, S. H., Nunez-Ramirez, R., Sorzano, C. O., Carazo, J. M. & Marabini, R. Image processing for electron microscopy single-particle analysis using XMIPP. *Nat. Protoc.* **3,** 977–990 (2008).

Acknowledgements

We thank E. Isono and H. Taguchi for yeast strains, D. Finley for antibody, K. Fukunaga and H. Kawamura for their assistance with earlier studies, and the members of the K. Tanaka lab for helpful discussions. This work was supported by JSPS KAKENHI (Grant Numbers 21025038 to C.-G.P. and Y. Saeki, 21000012 to S.M. and K.T., and 22657037, 24112008 to Y. Saeki) and Sonderforschungsbereich SFB-1035 to W.B.

Author contributions

C.-G.P., H.Y., A.T., T.K., H.T., A.K. and E.S. performed the experiments. C.-G.P. performed FCS/FCCS analysis. H.Y., A.T., T.K., H.T. and A.K. constructed yeast strains. E.S. performed cryo-EM analysis. C.-G.P., Y. Sako, S.M., H.Y., W.B., K.T. and Y. Saeki planned the studies and wrote the manuscript. All the authors commented on the manuscript.

Additional information

Supplementary Information accompanies this paper at http://www.nature.com/naturecommunications

Competing financial interests: The authors declare no competing financial interests.

Reprints and permission information is available online at http://npg.nature.com/reprintsandpermissions/

How to cite this article: Pack, C.-G. *et al.* Quantitative live-cell imaging reveals spatio-temporal dynamics and cytoplasmic assembly of the 26S proteasome. *Nat. Commun.* 5:3396 doi: 10.1038/ncomms4396 (2014).

Current Trends in Neurology

Original Communication

Segmental copy number loss of the PCSK6 gene in sporadic amyotrophic lateral sclerosis

Hidenori Sato[1], Shigeki Arawaka[1], Manabu Wada[1], Toru Kawanami[1], Fumiaki Tanaka[2], Gen Sobue[2], Mitsuru Emi[3] and Takeo Kato[1,*]

[1]Department of Neurology, Hematology, Metabolism, Endocrinology and Diabetology, Yamagata University, Faculty of Medicine, Yamagata, Japan; [2]Department of Neurology, Nagoya University School of Medicine, Nagoya, Japan. [3]Cancer Research Center, University of Hawaii, Honolulu, USA

ABSTRACT

Sporadic amyotrophic lateral sclerosis (SALS) is regarded as a multifactorial disease; both genetic and environmental factors may contribute to the pathogenesis of SALS. To identify a possible genetic change that confers risk for SALS, we conducted whole-genome screening of a copy-number variation (CNV) with a CNV beadchip and a high-density oligonucleotide tiling microarray, followed by real-time quantitative polymerase chain reaction (qPCR). In the 1.1- to 5.5- kb region within the gene encoding the proprotein convertase subtilisin/kexin type 6 (PCSK6) on the chromosome 15q26.3 subtelomere, we found a copy-number loss in a large proportion (8 of 11; 72%) of SALS patients. Subsequent tiling microarray validated the results and revealed the fine structure of segmental loss. qPCR analysis confirmed the copy-number loss in 13 out of 23 SALS patients, as compared with 7 out of 44 controls ($p = 0.0015$, Odds Ratio: 6.63, 95%CI: 1.89–25.72). The present study suggests that a segmental copy-number loss of the PCSK6 gene may play a role in the pathogenesis of SALS.

KEYWORDS: ALS, amyotrophic lateral sclerosis, copy-number variation, deletion, motor neuron, PCSK6, polymorphism, subtelomere

*Corresponding author: tkato@med.id.yamagata-u.ac.jp

1. INTRODUCTION

Amyotrophic lateral sclerosis (ALS) is an adult-onset, fatal neurodegenerative disease which is characterized neuropathologically by the degeneration of motor neurons in the brain and spinal cord. ALS has two subgroups: familial ALS (FALS) and sporadic ALS (SALS). FALS is a rare disease which is inherited in a Mendelian fashion, and several causal genes have been identified [1, 2]. The majority (90–98%) of ALS cases are SALS. Although the etiology of SALS remains to be determined, the "British motor neuron disease twin study" demonstrated the importance of a genetic component in SALS [3]. Genome-wide association studies using single nucleotide polymorphisms (SNPs) have been performed, and some SNPs showed significant associations with SALS [4-8]; however, others did not after correcting for multiple testing [9-11]. Moreover, even the SNPs significantly associated with SALS were not necessarily replicated in the later studies [11, 12].

Recently, copy-number variations (CNVs) have been reported as inter-individual genetic variations [13]. Several CNV abnormalities also seem to be significant in the etiology of sporadic and inherited diseases [reviewed in 14]. To identify a possible genetic change that confers risk for SALS, we performed a whole-genome analysis for CNV and found a copy number gain within the region of the isopentenyl diphosphate isomerase (IDI) genes in many patients with SALS [15]. Here, we report

another gene, the proprotein convertase subtilisin/kexin type 6 (PCSK6) gene, a segmental copy-number loss of which was significantly associated with SALS.

2. MATERIALS AND METHODS

2.1. Subjects

Fifty-nine patients with SALS were included in this study. These patients fulfilled the criteria for probable or definite ALS according to the 1994 El Escorial criteria [16]. 104 community-dwelling elderly individuals with no neurological diseases were randomly selected as control [17, 18]. No significant differences in the mean age (SALS/control = 60.6/70.0 years) or the ratio of men to women (SALS/control = 0.68/0.76) were observed between the two groups ($p > 0.05$ in both). One-hundred patients with Parkinson's disease were also included as disease-control [19]. DNA was extracted and purified from peripheral blood. Written informed consent for genetic analysis was obtained from all the subjects. The Medical Ethics Committee of Yamagata University, Faculty of Medicine approved the present study.

2.2. Screening with a whole-genome CNV beadchip

Whole-genome screening was conducted by using the deCODE-Illumina CNV beadchip (57K, i-select format, Illumina Infinium system, deCODE Genetics, Inc.). The CNV probes were designed to target CNV-rich regions of the whole genome, such as megasatellites, duplicons, unSNPable regions and CNVs registered in the Database of Genomic Variants. The regions contained 15,559 CNV segments, which cover 190 Mb or 6% of the human genome. CNV data were analyzed by using the DosageMiner program as described previously [20].

2.3. Analysis with high-density oligonucleotide tiling microarray

Agilent 400K high-density oligonucleotide tiling microarray assay was conducted on a CNV-enriched designed microarray (product #ID 02185, Agilent Technology, Inc.), which targets CNV-rich regions, median probe spacing 5 kb and average probe spacing 7 kb, in the whole-genome region. HapMap genome DNA [NA19000, JPN] was used as reference genome DNA. The intensity data were calculated by the ratio of the target genome intensities to the reference genome intensities. Abnormal copy number (loss or gain) was detected by deviation of probe $\log_2$ ratios exceeding a given threshold of 1 SD from the mean probe ratio [21, 22].

2.4. Real-time quantitative PCR (qPCR)

Copy numbers of the region of the PCSK6 gene on 15q26.3 were assayed by using TaqMan Gene Copy Number Assays of Life Technologies in basic qPCR according to the instructions of the manufacturer. The primers and probes were designed from the genomic sequence (hg18/Build 36) using proprietary web-based assay search tools (https://bioinfo.appliedbiosystems.com/genome-database/copy-number-variation.html). Each assay was run as a triplex TaqMan real-time qPCR reaction by using an FAM dye–based assay targeted to the region of the PCSK6 gene (Hs03912091_cn) and its flanking region (Hs0393814_cn) and a VIC dye–based assay for the reference gene, RNase P (PN 4316844 from Life Technologies). Each qPCR assay was performed in triplicate. Data were analyzed as described previously [23].

3. RESULTS

In search of a SALS-associated CNV, we performed whole-genome screening with the CNV beadchip for 11 SALS patients and 104 controls. We found

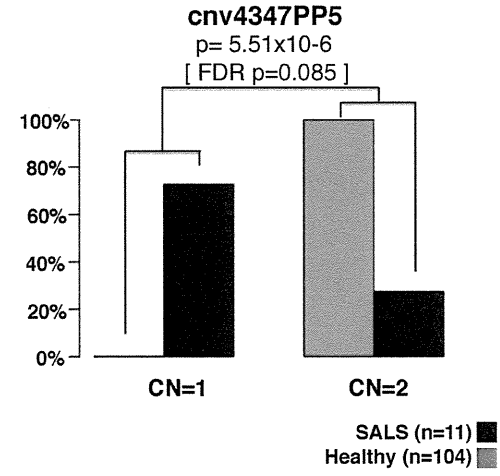

Figure 1. Frequency of copy number (CN) of the marker cnv4347PP5 in patients with sporadic amyotrophic lateral sclerosis (SALS) and healthy controls. The cnv4347PP5 is located in 3' exonic region of the PCSK6 gene. CNs were estimated by the deCODE-Illumina CNV beadchip (deCODE Genetics). CN=1: one copy, CN=2: two copies.

several CNV markers that were significantly associated with SALS. Among them, the marker cnv4347PP5 was located within the region of the PCSK6 gene on the 15q26.3 subtelomere. Eight of the 11 SALS patients showed a copy-number loss at the CNV marker on the PCSK6 gene region, as compared with 0 out of 104 control samples ($p = 5.51 \times 10^{-6}$ by logistic regression, $p < 0.1$ after false discovery rate correction) (Figure 1).

We then analyzed the structure of the copy-number change along the 15q26.3 subtelomeric region by using the high-density oligonucleotide tiling microarray in 50 SALS patients and 20 healthy controls. A segmental copy-number loss of 1.1–5.5 kb (Figure 2-A, Figure 2-B) in the 15q26.3 subtelomeric region was found in 15 of the SALS patients examined but in none of the control subjects ($p = 0.00629$, OR = 17.9, 95%CI: 1.02–315.15, Table 1).

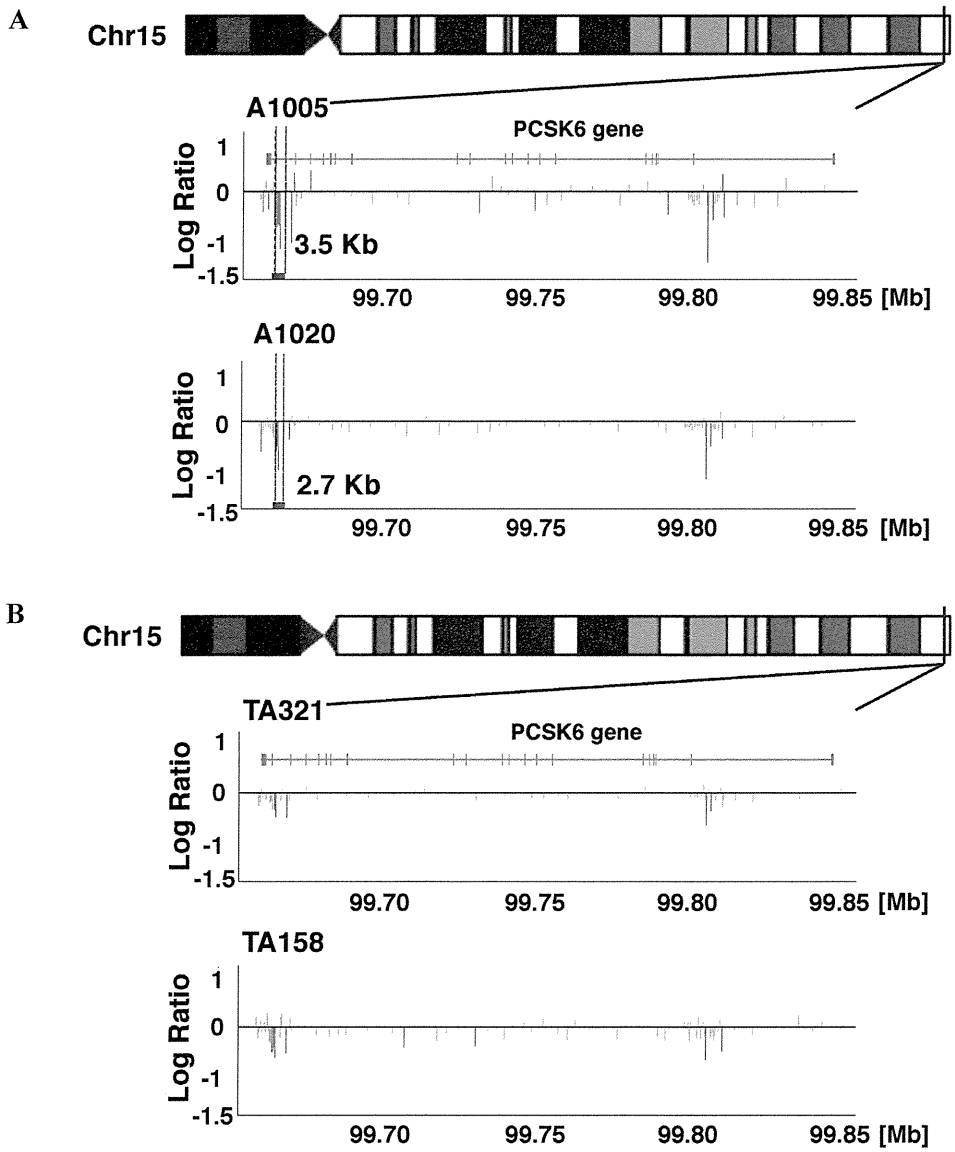

Figure 2. Fine structure of segmental copy-number loss in the PCSK6 gene region in two representative cases of SALS (A1005 and A1020) (A). The results of two healthy controls (TA321 and TA158) are shown in (B). The vertical red lines show average Log_2 Ratio. The vertical dot lines indicate the range of copy-number loss.

Table 1. Segmental copy number loss of PSCK6 gene in SALS and healthy subjects.

	CN = 1	CN = 2
SALS (n = 50)	15	35
Healthy (n = 20)	0	20

p=0.00629, OR=17.9 (1.02-315.15)

CN: estimated copy-number.
SALS: sporadic amyotrophic lateral sclerosis.

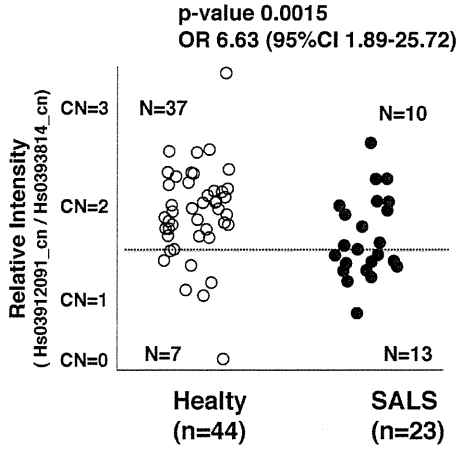

Figure 3. Quantitative PCR analysis for estimating the copy number in the region (Hs03912091_cn) of the PCSK6 gene. Its flanking region (Hs0393814_cn) is used as reference.

This region with copy-number loss contained the 3' exonic region of the PSCK6 gene (NM_138319 and NM_002570). A segmental copy-number loss in the PSCK6 gene was confirmed in 13 out of 23 (56%) SALS patients by basic real-time qPCR, as compared with 7 out of 44 controls (p = 0.0015, OR = 6.63, 95%CI: 1.89–25.72) (Figure 3). To test whether the copy-number change of the PSCK6 gene region was specific to SALS, we analyzed DNA from a total of 100 patients with Parkinson's disease. The results showed that no such change was observed in any cases of Parkinson's disease.

We have previously reported a copy-number gain in the region of the IDI genes on the 10p15.3 subtelomere in many patients with SALS [15]. We combined the present results (PCSK6 gene) with the previous results (IDI genes) designed using the same SALS-patients dataset. As shown

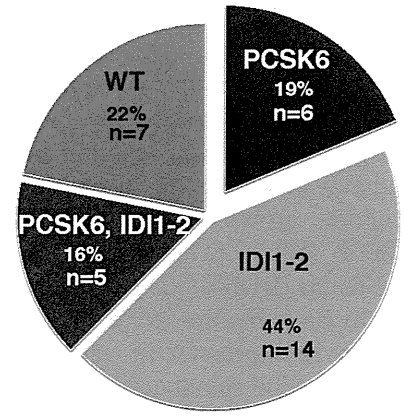

Figure 4. Frequency of copy-number loss of the PCSK6 gene region and/or copy-number gain of the IDI1-2 gene region in patients with SALS.
IDI1-2: isopentenyl diphosphate isomerase-1 and -2.

in Figure 4, among the 32 patients with SALS, 14 (44%) had a copy-number gain in the region of the IDI genes, and 6 (19%) showed a copy-number loss in the region of the PCSK6 gene. Twenty-five of 32 (78%) patients with SALS had a copy-number aberration of either gene or both.

4. DISCUSSION

The previously-reported genome-wide association studies on CNVs in SALS did not show a common CNV locus associated with SALS [24-26]. Those studies employed conventional platforms for genome-wide SNP genotyping, such as HumanHap300 and HumanHap550, which covered only 25% and 40% of the CNVs, respectively, resulting in the incapacity from capturing a large fraction of CNV [27]. CNVs not covered on the conventional SNP platforms were needed to do the examination [25]. We used a "CNV-targeted platform" that contains many CNV markers in the CNV-rich regions of the human genome. In the previous study, we reported a segmental copy-number gain in the IDI gene region on the 10p15.3 subtelomere in many SALS patients [15]. In the present study, we found another gene encoding PCSK6, the 3' region of which showed a segmental copy-number loss in 6 of 32 (19%) patients with SALS. 78% of the SALS patients had an aberration of either gene or both.

Many bioactive peptides are first synthesized as precursors that require proteolytic processing by the proprotein convertases [28]. The PCSK6

(also known as PACE4) gene, which is located on the chromosome 15q26.3 subtelomere, encodes a proprotein convertase that belongs to the subtilisin-like proprotein convertase family [29]. The PCSK6 protein has been reported to process several proteins, including neurotrophins (NTs), such as nerve growth factor (NGF) [30], neurotrophin 3 (NT3) [31], and brain-derived neurotrophic factor (BDNF) [31], from their latent precursors into biologically active products. The PCSK6 protein is expressed in various organs, including the brain and spinal cord [32, 33]. These NTs have been shown to regulate neuronal survival and death [34]. For example, NGF binds to its specific receptor (TrkA) and promotes neurite elongation and survival. On the other hand, proNGF, a precursor of NGF, binds to the p75 neurotrophin receptor (p75NTR) and induces apoptosis [34]. In the present study, a segmental copy-number loss was observed in the PCSK6 gene, suggesting that the function of PCSK6 as a proprotein convertase may be impaired. This may result in a decrease in the amount of biologically active, mature NTs and in an increase in the precursors of NTs. NTs and their receptors have been implicated as being involved in the pathological process of a mouse model of ALS and human SALS [35-39]. Indeed, a knockdown of p75NTR significantly delayed locomotor impairment and mortality in a mouse model of ALS [40, 41]. Taken together, it seems that neuronal death may be induced by the dysfunction of the PCSK6 gene in SALS.

CONCLUSION

In conclusion, we found a copy-number loss in the PCSK6 gene in a considerable number of patients with SALS. Further studies on the function of PCSK6 in motor neurons may contribute to the elucidation of the pathogenesis of SALS, leading to the identification of a novel therapeutic target of the disease.

ACKNOWLEDGEMENTS

This study was supported in part by Research on Measures for Intractable Diseases (ALS) from the Ministry of Health, Labour and Welfare of Japan.

CONFLICT OF INTEREST STATEMENT

There are no conflicts of interest.

REFERENCES

1. Lagier-Tourenne, C., Polymenidou, M. and Cleveland, D. W. 2010, Hum. Mol. Genet., 19, R46.
2. Maruyama, H., Morino, H., Ito, H., Watanabe, Y., Kinoshita, Y., Kamada, M., Nodera, H., Suzuki, H., Komure, O., Matsuura, S., Kobatake, K., Morimoto, N., Abe, K., Suzuki, N., Aoki, M., Kawata, A., Hirai, T., Kato, T., Ogasawara, K., Hirano, A., Takumi, T., Kusaka, H., Hagiwara, K., Kaji, R. and Kawakami, H. 2010, Nature, 465, 223.
3. Graham, A. J., MacDonald, A. M. and Hawkes, C. H. 1997, J. Neurol. Neurosurg. Psychiatry, 62, 562.
4. van Es, M. A., van Vught, P. W., Blauw, H. M., Franke, L., Saris, C. G., Andersen, P. M., Van Den Bosch, L., de Jong, S. W., van't Slot, R., Birve, A., Lemmens, R., de Jong, V., Baas, F., Shelhass, H. J., Sleegers, K., Van Broeckhoven, C., Wokke, J. H., Wijmenga, C., Robberecht, W., Veldink, J. H., Ophoff, R. A. and van den Berg, L. H. 2007, Lancet Neurol., 6, 869.
5. Dunckley, T., Huentelman, M. J., Craig, D. W., Pearson, J. V., Szelinger, S., Joshipura, K., Halperin, R. F., Samper, C., Jensen, K. R., Letizia, D., Hesteriee, S. E., Pestronk, A., Levine, T., Bertorini, T., Graves, M. C., Mozaffar, T., Jackson, C. E., Bosch, P., McVey, A., Dick, A., Barohn, R., Lomen-Hoerth, C., Rosenfeld, J., O'connor, D. T., Zhang, K., Crook, R., Ryberg, H., Hutton, M., Katz, J., Simpson, E. P., Mitsumoto, H., Bowser, R., Miller, R. G., Appel, S. H. and Stephan D. A. 2007, N. Engl. J. Med., 357, 775.
6. van Es, M.A., van Vught, P. W., Blauw, H. M., Franke, L., Saris, C. G., Van den Bosch, L., de Jong, S. W., de Jong, V., Baas, F., van't Slot, R., Lemmens, R., Schelhaas, H. J., Birve, A., Sleegers, K., Van Broeckhoven, C., Schymick, J. C., Traynor, B. J., Wokke, J. H., Wijmenga, C., Robberecht, W., Andersen, P. M., Veldink, J. H., Ophoff, R. A. and van den Berg, L. H. 2008, Nat. Genet., 40, 29.
7. Cronin, S., Berger, S., Ding, J., Schymick, J. C., Washecka, N., Hernandez, D. G., Greenway, M. J., Mradley, D. G., Traynor, B. J. and Hardiman, O. 2008, Hum. Mol. Genet., 17, 768.

8. van Es, M. A., Veldink, J. H., Saris, C. G., Blauw, H. M., van Vught, P. W., Birve, A., Lemmens, R., Shelhaas, H. J., Groen, E. J., Huisman, M. H., van der Kooi, A. J., de Visser, M., Dahlberg, C., Estrada, K., Rivadeneira, F., Hofman, A., Zwarts, M. J., van Doormaal, P. T., Rujescu, D., Strengman, E., Giegling, I., Muglia, P., Tomik, B., Slowik, A., Uitterlinden, A. G., Hendrick, C., Waibel, S., Meyer, T., Ludolph, A. C., Glass, J. D., Purcell, S., Cichon, S., Nöthen, M. M., Wichmann, H. E., Schreiber, S., Vermeulen, S. H., Klemeney, L. A., Wakko, J. H., Cronin, S., McLaughlin, R. L., Hardman, O., Fumoto, K., Pasterkamp, R. J., Meininger, V., Melki, J., Leigh, P. N., Shaw, C. E., Landers, J. E., Al-Chalabi, A., Brown Jr. R. H., Robberecht, W., Andersen, P. M., Ophoff, R. A. and van den Berg, L. H. 2009, Nat. Genet., 41, 1083.
9. Schymick, J. C., Scholz, S. W., Fung, H. C., Britton, A., Arepalli, S., Gibbs, J. R., Lombardo, F., Matarin, M., Kasperaviciute, D., Hemandez, D. G., Crews, C., Brujin, L., Rothstein, J., Mora, G., Restagno, G., Chi, A., Singleton, A., Hardy, J. and Traynor, B. J. 2007, Lancet Neurol., 6, 322.
10. Cronin, S., Tomik, B., Bradley, D. G., Slowik, A. and Hardiman, O. 2009, Eur. J. Hum. Genet., 17, 213.
11. Chiò, A., Schymick, J. C., Restagno, G., Scholz, S. W., Lombardo, F., Lai, S. L., Mora, G., Fung, H. C., Britton, A., Arepalli, S., Gibbs, J. R., Nalls, M., Berger, S., Kwee, L. C., Oddone, E. Z., Ding, J., Crews, C., Rafferty, I., Washecka, N., Hernandez, D., Ferrucci, L., Bandinelli, S., Guralnik, J., Macciardi, F., Torri, F., Lupoli, S., Chanock, S. J., Thomas, G., Hunter, D. J., Gieger, C., Wichmann, H. E., Calvo, A., Mutani, R., Battisini, S., Giannini, F., Caponnetto, C., Mancardi, G. L., La Bella, V., Valentino, F., Monsurrò, M. R., Tedeschi, G., Marinou, K., Sabatelli, M., Conte, A., Mandrioli, J., Sola, P., Salvi, F., Bartolomei, I., Siciliano, G., Carlesi, C., Orrell, R. W., Talbot, K., Simmons, Z., Connor, J., Pioro, E. P., Dunkley, T., Stephan, D. A., Kasperaviciute, D., Fisher, E. M., Jabonka, S., Sendtner, M., Beck, M., Bruijn, L., Rothstein, J., Schmidt, S., Singleton, A., Hardy, J. and Traynor, B. J. 2009, Hum. Mol. Genet., 18, 1524.
12. Fernández-Santiago, R., Sharma, M., Berg, D., lllig, T., Anneser, J., Meyer, T., Ludolph, A. and Gasser, T. 2011, Neurobiol. Aging, 32, 511.e1.
13. Redon, R., Ishikawa, S., Fitch, K. R., Feuk, L., Perry, G. H., Andrews, T. D., Flegler, H., Shapero, M. H., Carson, A. R., Chen, W., Cho, E. K., Dallaire, S., Freeman, J. L., Gratacòs, J. R., Huang, J., Kalaitzopoulos, D., Komura, D., MacDonald, J. R., Marshall, C. R., Mei, R., Montgomery, L., Nishimura, K., Okumura, K., Shen, F., Somerville, M. J., Tchinda, J., Valsesia, A., Woodwark, C., Yang, F., Zhang, J., Zerjai, T., Zhang, J., Armengol, L., Conrad, D. F., Estivill, X., Tyler-Smith, C., Carter, N. P., Aburatani, H., Lee, C., Jones, K. W., Scherer, S. W. and Hurles, M. E. 2006, Nature, 444, 444.
14. Lupski, J. R. 2007, Nat. Genet., 39, S43.
15. Kato, T., Emi, M., Sato, H., Arawaka, S., Wada, M., Kawanami, T., Katagiri, T., Tsuburaya, K., Toyoshima, I., Tanaka, F., Sobue, G. and Matsubara, K. 2010, Biochem. Biophys. Res. Commun., 402, 438.
16. Brooks B. R. 1994, J. Neurol. Sci., 124 (Suppl.), 96.
17. Nagasawa, H., Wada, M., Arawaka, S., kawanami, T., Kurita, K., Daimon, M., Adachi, M., Hosoya, T., Emi, M., Muramatsu, M. and Kato, T. 2007, Eur. J. Neurol., 14, 428.
18. Iseki, C., Kawanami, T., Nagasawa, H., Wada, M., Koyama, S., Kikuchi, K., Arawaka, S., Kurita, K., Daimon, M., Mori, E. and Kato, T. 2009, J. Neurol. Sci., 277, 54.
19. Arawaka, S., Wada, M., Goto, S., Karube, H., Sakamoto, M., Ren, C-H., Koyama, S., Nagasawa, H., Kimura, H., Kawanami, T., Kurita, K., Tajima, K., Daimon, M., Baba, M., Kido, T., Saino, S., Goto, K., Asao, H., Kitanaka, C., Takashita, E., Hongo, S., Nakamura, T., Kayama, T., Suzuki, Y., Kobayashi, K., Katagiri, T., Kurokawa, K., Kurimura, M., Toyoshima, I., Tsuchiya, K., Iwatsubo, T., Muramatsu, M., Matsumine, H. and Kato T. J. Neurosci., 2006, 26, 9227.

20. Stefansson, H., Rujescu, D., Cichon, S., Pletilälnen, O. P., Ingason, A., Steinberg, S., Fossdai, R., Sigurdsson, E., Sigmundsson, T., Bulzer-Voskamp, J. E., Hansen, T., Jakobsen, K. D., Mugila, P., Francks, C., Matthews, P. M., Gylfason, A., Halldorsson, B. V., Gudbjartsson, D., Thorgeirsson, T. E., Sigurdsson, A., Jonasdottir, A., Jonasdottir, A., Bjornsson, A., Mattiasdottir, S., Blondal, T., Haraldsson, M., Magnusdottir, B. B., Giegling, I., Möller, H. J., Hartmann, A., Shianna, K. V., Ge, D., Need, A. C., Crombie, C., Fraser, G., Walker, N., Lonnqvist, J., Suvisaari, J., Tuulio-Henriksson, A., Paunio, T., Toulopoulou, T., Bramon, E., Di Forti, M., Murray, R., Ruggeri, M., Vassos, E., Tosato, S., Walshe, M., Li, T., Vasilescu, C., Mühleisen, T. W., Wang, A. G., Ullum, H., Djurovic, S., Melle, I., Olessen, J., Kiemeney, L. A., Franke, B., Sabatti, C., Freimer, N. B., Gulcher, J. R., Thorsteinsdottir, U., Kong, A., Andreassen, O. A., Ophoff, R. A., Georgi, A., Rietschel, M., Werge, T., Petursson, H., Goldstein, D. B., Nöthen, M. M., Peltonen, L., Collier, D. A., St. Clair, D. and Stefansson, K. 2008, Nature 455, 232.
21. de Smith, A. J., Tsalenko, A., Sampas, N., Scheffer, A., Yamada, N. A., Tsang, P., Ben-Dor, A., Yakhini, Z., Ellis, R. J., Bruhn, L., Laderman, S., Froguel, P. and Blakemore, A. I. 2007, Hum. Mol. Genet., 16, 2783.
22. Sharp A. J., Hansen S., Selzer R. R., Regan, R., Hurst, J. A., Stewart, H., Price, S. M., Blair, E., Hennekam, R. C., Fitzpatrick, C. A., Segraves, R., Richmond, T. A., Guiver, C., Albertson, D. G., Pinkel, D., Els, P. S., Schwartz, S., Knight, S. J. and Eichler, E. E. 2006, Nat. Genet., 38, 1038.
23. Livak, K. J. and Schmittgen T. D. 2001, Methods, 25, 402.
24. Blauw, H. M., Veldink, J. H., van Es, M. A., van Vught, P. W., Saris, C. G., van der Zwaag, B., Franke, L., Burbach, J. P., Wokke, J. H., Ophoff, R. A. and van den Berg, L. H. 2008, Lancet Neurol., 7, 319.
25. Cronin, S., Blauw, H. M., Veldink, J. H., van Es, M. A., Ophoff, R. A., Bradley, D. G., van den Berg, L. H. and Hardman, O. 2008, Hum. Mol. Genet., 17, 3392.
26. Wain L. V., Pedroso I., Landers J. E., Breen, G., Shaw, C. E., Leigh, P. N., Brown, R. H., Tobin, M. D. and Al-Chalabi A. 2009, PLoS ONE, 4, e8175.
27. Cooper, G. M, Zerr, T., Kidd, J. M., Eichler, E. E. and Nickerson, D. A. 2008, Nat. Genet., 40, 1199.
28. Steiner, D. F. 1998, Curr. Opin. Chem. Biol., 2, 31.
29. Kiefer, M. C., Tucker, J. E., Joh, R., Landsberg, K. E., Saltman, D. and Barr, P. J. 1991, DNA Cell. Biol., 10, 57.
30. Seidah, N. G., Benjannet, S., Pareek, S., Savaria, D., Hamelin, J., Goulet, B., Laliberte, J., Lazure, C., Chrétien, M. and Murphy, R. A. 1996, Biochem. J., 314, 951.
31. Seidah, N. G., Benjannet, S., Pareek, S., Chretien, M. and Murphy, R. A. 1996, FEBS Lett., 379, 247.
32. Zheng, M., Seidah, N. G. and Pintar J. E. 1997, Dev. Biol., 181, 268.
33. Hajebrahimi, Z., Mowla, S. J., Movahedin, M. and Tavallaei M. 2008, Neurosci. Lett., 441, 261.
34. Lee, R., Kermani, P., Teng, K. K. and Hempstead, B. L. 2001, Science, 294, 1945.
35. Anand P., Parrett A., Martin J., Zeman, S., Foley, P., Swash, M., Leigh, P. N., Cedarbaum, J. M., Lindsay, R. M., Williams-Chestnut, R. E. and Sinicropi, D. V. 1995, Nat. Med., 1, 168.
36. Küst, B. M., Copray, J. C. V. M., Brouwer, N., Troost, D. and Boddeke, H. W. G. M. 2002, Exp. Neurol., 177, 419.
37. Barbeito, L. H., Pehar, M., Cassina, P., Vargas, M. R., Peluffo, H., Viera, L., Estévez, A. G. and Beckman, J. S. 2004, Brain Res. Rev., 47, 263.
38. Copray, J. C., Jaarsma, D., Küst, B. M., Bruggeman, R. W., Mantingh, I., Brouwer, N. and Boddeke, H. W. 2003, Neuroscience, 116, 685.
39. Pehar, M., Cassina, P., Vargas, M. R., Castellanos, R., Vlera, L., Beckman, J. S., Estévez, A. G. and Barbeito, L. 2004, J. Neurochem., 89, 464.
40. Küst, B. M., Brouwer, N., Mantingh, I. J., Boddeke H. W. and Copray J. C. 2003, Amyotroph. Lateral Scler. Other Motor Neuron Disord., 4, 100.
41. Turner, B. J., Cheah, I. K., Macfarlane, K. J., Lopes, E. C., Petratos, S., Langford, S. J. and Cheema, S. S. 2003, J. Neurochem., 87, 752.

Molecular Brain

RESEARCH Open Access

SIRT1 overexpression ameliorates a mouse model of SOD1-linked amyotrophic lateral sclerosis via HSF1/HSP70i chaperone system

Seiji Watanabe[1,3†], Natsumi Ageta-Ishihara[2†], Shinji Nagatsu[3,4†], Keizo Takao[5,6,9], Okiru Komine[1,3], Fumito Endo[1,3], Tsuyoshi Miyakawa[5,6,7,9], Hidemi Misawa[4], Ryosuke Takahashi[8,9], Makoto Kinoshita[2,9*] and Koji Yamanaka[1,3,9*]

Abstract

Background: Dominant mutations in superoxide dismutase 1 (SOD1) cause degeneration of motor neurons in a subset of inherited amyotrophic lateral sclerosis (ALS). The pathogenetic process mediated by misfolded and/or aggregated mutant SOD1 polypeptides is hypothesized to be suppressed by protein refolding. This genetic study is aimed to test whether mutant SOD1-mediated ALS pathology recapitulated in mice could be alleviated by overexpressing a longevity-related deacetylase SIRT1 whose substrates include a transcription factor heat shock factor 1 (HSF1), the master regulator of the chaperone system.

Results: We established a line of transgenic mice that chronically overexpress SIRT1 in the brain and spinal cord. While inducible HSP70 (HSP70i) was upregulated in the spinal cord of SIRT1 transgenic mice (PrP-Sirt1), no neurological and behavioral alterations were detected. To test hypothetical benefits of SIRT1 overexpression, we crossbred PrP-Sirt1 mice with two lines of ALS model mice: A high expression line that exhibits a severe phenotype ($SOD1^{G93A}$-H) or a low expression line with a milder phenotype ($SOD1^{G93A}$-L). The *Sirt1* transgene conferred longer lifespan without altering the time of symptomatic onset in $SOD1^{G93A}$-L. Biochemical analysis of the spinal cord revealed that SIRT1 induced HSP70i expression through deacetylation of HSF1 and that $SOD1^{G93A}$-L/PrP-Sirt1 double transgenic mice contained less insoluble SOD1 than $SOD1^{G93A}$-L mice. Parallel experiments showed that *Sirt1* transgene could not rescue a more severe phenotype of $SOD1^{G93A}$-H transgenic mice partly because their HSP70i level had peaked out.

Conclusions: The genetic supplementation of SIRT1 can ameliorate a mutant SOD1-linked ALS mouse model partly through the activation of the HSF1/HSP70i chaperone system. Future studies shall include testing potential benefits of pharmacological enhancement of the deacetylation activity of SIRT1 after the onset of the symptom.

Keywords: Sirtuin 1 (SIRT1), Cu/Zn-superoxide dismutase (SOD1), Heat shock factor 1 (HSF1), Heat shock protein (HSP), Amyotrophic lateral sclerosis (ALS), Systematic behavioral screening

* Correspondence: kinoshita.makoto@c.mbox.nagoya-u.ac.jp; kojiyama@riem.nagoya-u.ac.jp
†Equal contributors
[2]Department of Molecular Biology, Division of Biological Sciences, Nagoya University Graduate School of Science, Furo-cho, Chikusa, Nagoya 464-8602, Japan
[1]Department of Neuroscience and Pathobiology, Research Institute of Environmental Medicine, Nagoya University, Furo-cho, Chikus, Nagoya 464-8601, Japan
Full list of author information is available at the end of the article

Background

Pathological protein aggregation is a major hallmark of neurodegenerative diseases including amyotrophic lateral sclerosis (ALS), Parkinson's disease, Alzheimer's disease and polyglutamine diseases [1]. In ALS, approximately 10% is inherited and about 20% of the inherited ALS are caused by dominant mutations in the gene encoding Cu/Zn-superoxide dismutase (SOD1) [2]. Many of ALS causative SOD1 mutants retain the enzymatic activity for catalyzing superoxide anion to hydrogen peroxide and deletion of wild-type SOD1 from mice does not cause ALS phenotype, suggesting that SOD1 mutants provoke motor neuron degeneration through "gain of toxic function" mechanisms [3]. It has been suggested that altered conformations of mutant SOD1 proteins are linked to the toxicity [4]. Recent studies demonstrated that accumulation of misfolded SOD1 proteins is not only specific to SOD1-related familial ALS but also involved in a subset of sporadic ALS [5,6].

Chaperone system is a major cytoprotective mechanism against proteotoxic stresses. Unfolded or misfolded proteins are restored to their proper conformations with the help of heat shock proteins (HSPs) including HSP110/105, constitutive and inducible HSP70s (HSC70, HSP70i). HSP110/105, HSP70i, and HSP40 directly bind to mutant SOD1 and facilitate the clearance of SOD1 through the ubiquitin-proteasome pathway [7–9], suggesting that HSPs are involved in the neuroprotective mechanisms against SOD1-mediated neurodegeneration. Indeed, HSP70i co-expression in motor neurons substantially inhibits the SOD1-aggregation and improves the cell viability [10]. Moreover, HSP70i is also effective against other neurodegenerative diseases, such as Parkinson's disease [11] and Alzheimer's disease [12]. These data suggest that the induction of HSPs is a promising therapeutic strategy for neurodegenerative diseases including ALS.

Upon exposure to proteotoxic stresses, heat shock factor 1 (HSF1) forms a trimer, translocates to the nucleus, binds to regulatory elements of DNA, and upregulates a set of genes including HSP70i whose products constitute the chaperone system [13]. Deacetylation of HSF1, which is mediated partly by a sirtuin family deacetylase SIRT1, prolongs its binding to the heat shock promoters [14]. Recent studies have demonstrated beneficial effects of resveratrol, which is considered to potentiate the sirtuin cascade, on SOD1-ALS models [15,16]. Given the pleiotropic effect of resveratrol through non-sirtuin targets, the role of SIRT1 in motor neuron degeneration is to be examined. However, the effect of genetic supplementation of SIRT1 in ALS mice has never been directly tested.

On the basis of the above background, in this study we establish transgenic mouse lines that express SIRT1 in the central nervous system (CNS) under control of the murine prion promoter (PrP). We find that modest overexpression of SIRT1 alone does not cause neurological and behavioral alterations. To test the effects of SIRT1 overexpression, we crossbred the line with either of the two lines of transgenic mice which express a high and a low dose of the toxic $SOD1^{G93A}$ polypeptide that recapitulate selective motor neuron degeneration. We find that SIRT1 overexpression consistently endows partial rescue effects with the milder ALS model with the lower dose of $SOD1^{G93A}$. Biochemical analysis of the spinal cord extracts reveals upregulation of HSP70i and reduced aggregation of $SOD1^{G93A}$ in the $SOD1^{G93A}$/PrP-Sirt1 mice, corroborating the beneficial role of SIRT1 partly through activating the HSF1/HSP70i system.

Results

Generation of a prion promoter-driven *Sirt1* transgenic mouse

We generated transgenic mice that chronically express mouse SIRT1 in the CNS under control of the murine prion gene promoter (Figure 1A) (see Methods). The founder transgenic mice were backcrossed with wild-type C57BL/6 J mice, and a transgenic line with the highest SIRT1 protein level in the brain was selected. The offspring was further backcrossed for more than ten generations and established a transgenic line that gave consistent pan-neural expression of exogenous SIRT1. We compared the heterozygous *Sirt1* transgenic mice (PrP-Sirt1) with their non-transgenic littermates for the expression level of SIRT1 protein in the brain and spinal cord. Immunoblot analyses for SIRT1 confirmed the clear induction of active SIRT1 in the brain and spinal cord of PrP-Sirt1 mice (Figure 1B) (Additional file 1: Figure S1). In the PrP-Sirt1 mouse spinal cord, the expression level of SIRT1 protein was about three-fold higher than the one in the non-transgenic littermates. The lifespan of the PrP-Sirt1 mice was comparable to that of their non-transgenic littermates (Figure 1C).

Chronic overexpression of SIRT1 in the CNS does not affect the behavior of mice

As a means of unbiased screening for potential neurological alterations, PrP-Sirt1 mice were subjected to a battery of physical and behavioral examinations. Overall, PrP-Sirt1 transgenic and non-transgenic male littermates (n = 15 and 20, tested at 5–9 months of age) did not differ in their physical and behavioral indices quantified, except for a few minor items (Table 1 and Additional file 1: Figure S3-S17. The raw data are accessible at the Mouse Phenotype Database, http://www.mousephenotype.org/). These findings indicate that chronic overexpression of SIRT1 in the mouse CNS does not cause major physical or neuropsychiatric alterations up to that age.

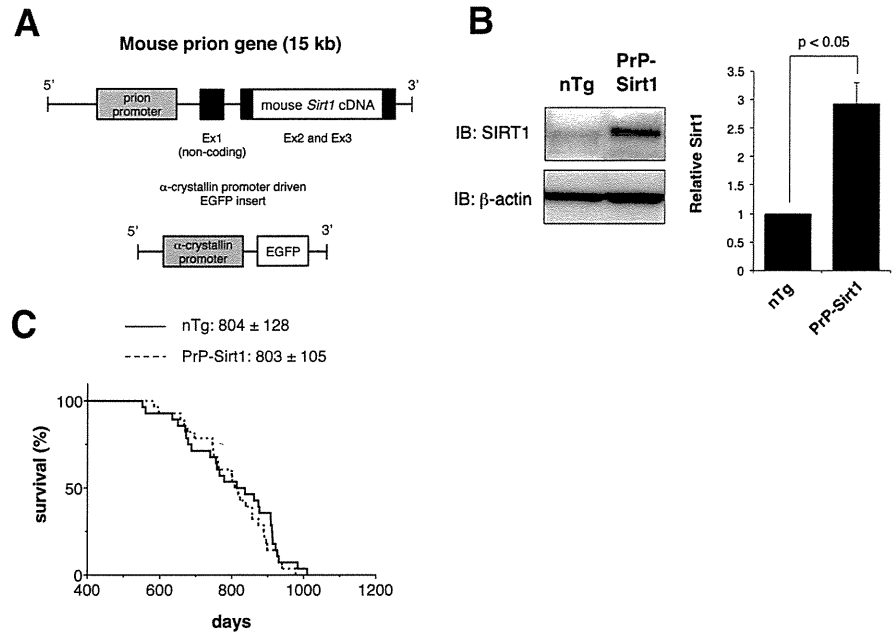

Figure 1 Generation of a line of transgenic mice that overexpress SIRT1 (PrP-Sirt1). (A) Schematic diagram of transgenes used to generate PrP-Sirt1 founder mice. Full-length mouse *Sirt1* cDNA was subcloned into the MoPrP (mouse prion promoter)-vector [37]. The non-coding portion of exon 2 and 3, and the *Sirt1* cDNA insert (with its own start and stop codon) were fused into one exon. The linearized transcription unit was co-injected with a visual marker, α-crystallin promoter-driven enhanced green fluorescent protein (EGFP) cDNA. **(B)** SIRT1 expression in PrP-Sirt1 and non-transgenic (nTg) mouse spinal cord. The expression level of Sirt1 was quantified in three independent experiments and shown as mean ± standard error of the mean (SEM). The data was analyzed by Student's t-test. **(C)** Survival curve of the PrP-Sirt1 and nTg mice plotted over time (n = 28 each). Mean survival time (days) was shown with standard deviation (SD).

Endogenous SIRT1 is upregulated in the spinal cord of SOD1^{G93A} and SOD1^{G37R} transgenic mouse

We have previously reported that HSP70i is induced in the spinal cord of SOD1^{G93A} transgenic mouse [9]. To test the possible involvement of SIRT1 in the induction of HSP70i, we investigated the expression level of SIRT1 in the spinal cords of high expression line of SOD1^{G93A} mouse (SOD1^{G93A}-H) and SOD1^{G37R} transgenic mouse which expresses human SOD1 gene carrying another ALS-linked mutation [17,18]. SIRT1 and HSP70i were clearly upregulated toward the end stage (5 months of age) of SOD1^{G93A}-H mice (Figure 2A). In SOD1^{G93A}-H/PrP-Sirt1 double transgenic mice, the level of HSP70i was not different from that of SOD1^{G93A}-H mice (Figure 2A) (Additional file 1: Figure S1), suggesting that the induction of HSP70i had peaked out. Similarly, SIRT1 was upregulated from around the symptomatic onset (10 months of age) to the end stage (13 months of age) in the spinal cords of SOD1^{G37R} mice (Figure 2B). HSP70i was induced only at the end stage, when HSP90 and HSP110/105 were downregulated (Figure 2C), consistent with our previous results on the expression of HSPs in SOD1^{G93A} mice [9].

SIRT1 overexpression extends lifespan of the transgenic mouse expressing low copy of SOD1^{G93A}

To examine putative beneficial effects of SIRT1 overexpression on the neurotoxicity by mutant SOD1, we cross-bred the PrP-Sirt1 mice with two lines of SOD1^{G93A} transgenic mice; SOD1^{G93A}-H and SOD1^{G93A}-L with a lower copy number . SOD1^{G93A}-L mice express *SOD1*^{G93A} transgene approximately 60% of SOD1^{G93A}-H mice (Additional file 1: Figure S2) and survive about 30 days longer on average (Figure 3A). We found that SIRT1 overexpression significantly extended the lifespan of SOD1^{G93A}-L mice (Figure 3A) without altering the onset of disease (Figure 3B). In contrast, SIRT1 did not give any beneficial effects on the lifespan (Figure 3C) and the disease onset of SOD1^{G93A}-H mice (Figure 3D). The disease progression was analyzed by dividing the total disease duration into the early and late phases (Figure 4A). SIRT1 extended the total disease duration in SOD1^{G93A}-L mice (74.6 ± 18.8 days for SOD1^{G93A}-L/PrP-Sirt1; 63.2 ± 12.6 days for SOD1^{G93A}-L) (Figure 4B). Interestingly, while the early phase duration was slightly reduced (34.3 ± 9.32 days for SOD1^{G93A}-L/PrP-Sirt1; 42.0 ± 10.3 days for SOD1^{G93A}-L) (Figure 4C), further

Table 1 Summary of systematic behavioral tests for PrP-Sirt1 mice in comparison with wild-type littermates

Tests	Mental/physical activities	Indices measured	Alteration from wild type
		(inexhaustive)	PrP-Sirt1
General health and neurological screening	General health	Body weight	↓
(Additional file 1: Figure S3)		Rectal temperature	→
		Grip strength	→
		Hanging persistence	↓
Light/dark transition test	Exploratory activity	Distance traveled in the light chamber	→
(Additional file 1: Figure S4)	Light avoidance	Distance traveled in the dark chamber	→
		Latency to the first entry to the light chamber	→
		Time stayed in the light chamber	→
		Number of transitions between chambers	↓
Open field test	Exploratory activity	Distance traveled	↑
(Additional file 1: Figure S5)	Avoidance from open space	Center time	→
	Anxiety-like behavior	Vertical activity	→
		Stereotypic counts	→
Elevated plus maze test	Exploratory activity	Distance traveled	→
(Additional file 1: Figure S6)	Height avoidance	Entries into open arms	→
		Number of entries	→
		Time stayed on open arms	→
Acoustic startle response	Startle reflex to loudness	Ampliture of body motion	→
(Additional file 1: Figure S7A)			
Prepulse inhibition (PPI) test	Sensorimotor gating	Decrement of startle amplitude	→
(Additional file 1: Figure S7B)			
Porsolt forced swim test	Despair-like behavior	Latency to immobility	→
(Additional file 1: Figure S8)			
Home cage monitoring	Diurnal cycle of locomotor activity	Activity level (distance traveled)	→
(Additional file 1: Figure S9)	Social behavior	Mean number of particles	→
Social interaction test	Social behavior, anxiety-like behavior	Distance traveled	→
(1 chamber, stranger pair)		Number of contacts	→
(Additional file 1: Figure S10)		Total duration of active contacts	→
		Mean contact duration	→
		Total duration of contacts	→
Social interaction test	Social behavior, anxiety-like behavior	Time spent with novel stranger	↓ (Step 2)
(3 chamber, 1–2 caged strangers)			
(Additional file 1: Figure S11)		Distance traveled	→
Rota-rod test	Motor coordination/learning	Latency to fall	→
(Additional file 1: Figure S12)			
Gait analysis	Mechanics of limb movement	Limb positions and timings	→ (front step angle)
(Additional file 1: Figure S13)			↑ (hind step angle)
Hot plate test	Aversive response to noxious stimulus	Latency to limb withdrawal	→

Table 1 Summary of systematic behavioral tests for PrP-Sirt1 mice in comparison with wild-type littermates *(Continued)*

(Additional file 1: Figure S14)			
Tail suspension test	Behavioral despair	Latency to immobility	→
(Additional file 1: Figure S15)			
Barnes maze	Spatial memory	Time spent around each hole	→
(Additional file 1: Figure S16)			
Fear conditioning test	Fear memory	Conditioning	→
(Additional file 1: Figure S17)		Contextual testing	→
		Cued test with altered context	→

Comparative table of behavioral test results with PrP-Sirt1 and wild-type littermate C57BL/6 J mice. Symbols: →, no significant difference; ↑↓, statistically significant increase and decrease as compared with wild-type control mice. N.D., not determined.

extension was observed in the late-phase (40.3 ± 20.2 days for $SOD1^{G93A}$-L/PrP-Sirt1; 21.2 ± 8.92 days for $SOD1^{G93A}$-L) (Figure 4D). These data indicate that SIRT1 overexpression was sufficient to slow the disease progression of $SOD1^{G93A}$-L mice, but not of $SOD1^{G93A}$-H mice.

SIRT1 overexpression causes deacetylation of HSF1, upregulation of HSP70i, and reduction of misfolded $SOD1^{G93A}$

To assess whether the disease progression is correlated with the deactylation level of HSF1 and/or the expression of HSP70i, we performed immunoprecipitation and immunoblot analysis. In a 5-month-old PrP-Sirt1 mouse spinal cord, the ratio of acetylated HSF1 over total HSF1 was significantly less and the level of HSP70i was significantly higher than those of the littermate (Figure 5A and B). These data suggest direct or indirect activation of the HSF1/HSP70i pathway by SIRT1 overexpression. Despite SIRT1 overexpression, however, HSP70i was not further upregulated in $SOD1^{G93A}$-H, $SOD1^{G93A}$-L mice at the end stage (Additional file 1: Figure S1), implying that HSP70i had been peaked out. To test the putative beneficial effects of SIRT1 overexpression against $SOD1^{G93A}$-mediated proteotoxicity, we measured disease-related dimerization of mutant SOD1. Previous studies showed that mutant SOD1 forms Triton X-100 insoluble and sodium dodecyl sulfate (SDS)-resistant dimer in the spinal cord of transgenic mice at symptomatic phase whose accumulation is inversely correlated with proteasome and chaperone activities [8,19]. We found that the dimerized SOD1 (approximately 40 kDa) in the spinal cord of a $SOD1^{G93A}$-L/PrP-Sirt1 mouse was less than that of a littermate $SOD1^{G93A}$-L mouse (Figure 5C). Since SDS-resistant SOD1 dimer was not detected in a presymptomatic $SOD1^{G93A}$-L mouse (60 days of age) (Figure 5C, left panel), HSP70i induced through the SIRT1/HSF1 pathway might reduce the accumulation of the toxic SOD1 dimers after the onset of the symptom. These findings suggest that the SIRT1/HSF1/HSP70i pathway contributes to the reduction of toxic misfolded and/or aberrantly dimerized species of SOD1, which accumulate in the late phase of the disease.

Discussion

In this study, we established a line of transgenic mice that chronically overexpress SIRT1 in the brain and spinal cord. As expected, overexpression of SIRT1 gave partial rescue effect on $SOD1^{G93A}$ mice. Supplementation of SIRT1 in the CNS slowed the disease progression and extended the lifespan of $SOD1^{G93A}$-L mice with a reduction of misfolded/aggregated SOD1 presumably through the activation of the HSF1/HSP70i pathway.

Previous reports from other groups showed that SIRT1 overexpression causes deficits in reference memory in the novel object recognition test [20], voluntary movement in the open field test, and motor coordination in the rotating rod test [21]. In contrast, we detected no significant neurological or behavioral differences between PrP-Sirt1 mice and their non-transgenic littermates with a few minor exceptions (Table 1, Additional file 1: Figure S3-S17). The discrepancy might be due to the transgene constructions, genomic position effects, and epigenetic factors that affect the levels and spatiotemporal patterns of expression. Our PrP-Sirt1 mice with minimal neurological deficits are suitable for testing the effects of SIRT1 supplementation on various models of neurological disorders. In fact, their remarkable resistance against cerebral hypoperfusion has been demonstrated with a bilateral carotid artery stenosis model [22].

The beneficial role of SIRT1 has been demonstrated in various neurodegenerative disease models. Neuroprotective effects of SIRT1 have been reported in Huntington's disease [23,24], Parkinson's disease [25], Alzheimer's disease [26,27], and spinal and bulbar muscular atrophy [28]. In this study, we demonstrated that SIRT1 overexpression has partial protective effects on a mouse ALS model. Previous studies showed that resveratrol, an activator of SIRT1, extended the lifespan of $SOD1^{G93A}$ mice [15,16]. However, given the pleiotropic effects of resveratrol through other target proteins, our results provide

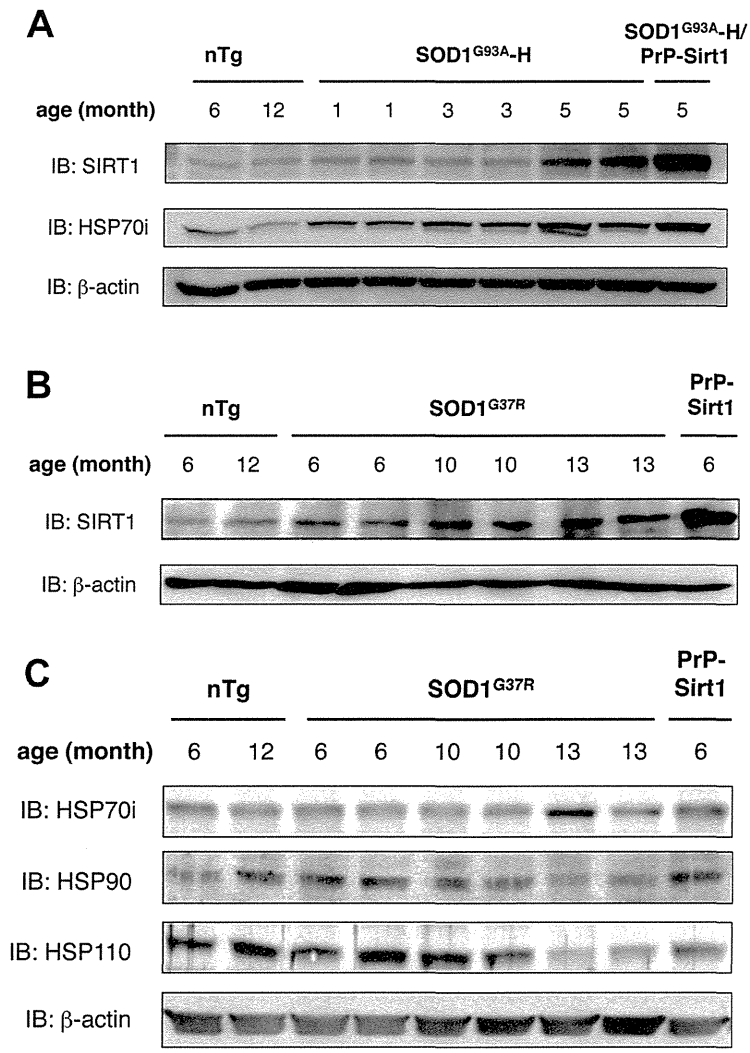

Figure 2 Expression of endogenous SIRT1 and the major heat shock proteins in the spinal cord of SOD1^{G93A}, SOD1^{G37R} or SIRT1 transgenic mice. (A) Endogenous SIRT1 and HSP70i were upregulated in high copy SOD1^{G93A} mouse (SOD1^{G93A}-H) spinal cord. A representative immunoblot image for SIRT1 and HSP70i in the lumbar spinal cord of SOD1^{G93A}-H, SOD1^{G93A}-H and PrP-Sirt1 double transgenic (SOD1^{G93A}-H/PrP-Sirt1), or non-transgenic (nTg) mice at designated age. Each lane contained 30 μg total protein and the similar results were obtained from three independent experiments. **(B)** Endogenous SIRT1 was upregulated in SOD1^{G37R} mouse spinal cord. A representative immunoblot image for SIRT1 in the lumbar spinal cord of SOD1^{G37R}, PrP-Sirt1, or nTg mice at designated age. Each lane contained 20 μg total protein and the similar results were obtained from three independent experiments. **(C)** HSP70i was modestly induced in SOD1^{G37R} mouse spinal cord. Representative immunoblot images for HSP70i, HSP90, and HSP110 in the same lumber spinal cord homogenates as in **(B)**. Each lane contained 30 μg total protein and the similar results were obtained from three independent experiments.

the first direct evidence for the contribution of SIRT1 to the alleviation of neurodegeneration in the ALS model.

Our findings suggest that the beneficial effects of SIRT1 depend at least in part on the HSF1/HSP70i pathway. This is consistent with a previous study demonstrating that HSF1 overexpression is partially protective against SOD1-mediated toxicity through the induction of HSP70i and αB-crystallin [29]. On the other hand, it should be noted that this study does not exclude possible involvement of other downstream effectors of SIRT1, such as PGC-1α , or p53, in the neuroprotective effects.

HSP70i reduces Triton X-100-insoluble SOD1 species (Figure 5C) [8] and exogenously delivered HSP70i extends the lifespan of SOD1^{G93A} mice [30]. Although it is unknown whether the mutant SOD1 proteins are refolded, degraded or both in each case, these data suggest the reduction of toxic SOD1 species contributes to the amelioration of SOD1-linked ALS model mice by inducing HSP70i. Since endogenous chaperone system was not sufficiently activated in SOD1-linked ALS model mice (Figure 2C) [9], supplementation of HSPs would be a promising means to cope with the proteotoxicity of

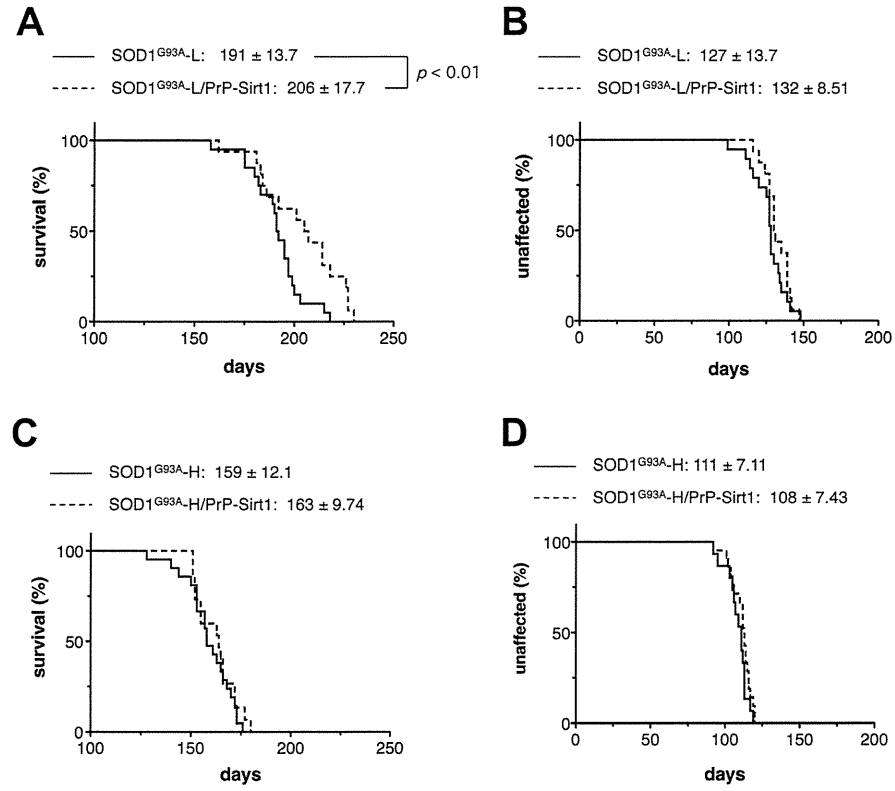

Figure 3 Effects of SIRT1 overexpression on the lifespan and onset of non-transgenic, and high and low copy SOD1^{G93A} transgenic mice. (A and B) Survival **(A)** and the onset of the symptom, determined by weight reduction **(B)** of SOD1^{G93A}-L (n = 19) and SOD1^{G93A}-L/PrP-Sirt1 (n = 16) mouse cohort plotted over time. **(C and D)** Survival **(C)** and the onset of the symptom **(D)** of SOD1^{G93A}-H (n = 21) and SOD1^{G93A}-H/PrP-Sirt1 (n = 15) mouse cohort plotted over time. The data were analyzed by log-rank test and the average onset and survival time are shown with SD.

mutant SOD1. Another study showed that HSP70i overexpression does not ameliorate the symptom and pathology of SOD1^{G93A}, SOD1^{G37R}, and SOD1^{G85R} transgenic mouse lines [31]. We speculate that the differences come from the severity of the models. As we demonstrated, SIRT1 overexpression was effective for the rescue of SOD1^{G93A}-L but not of SOD1^{G93A}-H (Figure 3), whose levels of HSP70i in the end stage were comparable (Additional file 1: Figure S1). These findings suggest that the refolding capacity of HSP70i against the toxicity of mutant SOD1 is limited, especially in the presence of excess amounts of misfolded proteins by overexpression of transgene.

We have previously demonstrated that E6-associated protein (E6-AP), a dual function steroid hormone receptor coactivator and ubiquitin-protein ligase, is involved in SOD1 aggresome degradation and suppresses mutant SOD1-mediated toxicity [32]. Interestingly, E6-AP ubiquitinates the misfolded proteins that are bound to HSC70 [33], and co-expression of E6-AP and HSC70 gives more potent neuroprotection [32]. It is also known that C-terminus of HSP70-interacting protein (CHIP) is involved in misfolded protein degradation through the ubiquitin-proteasome system [34,35]. These observations suggest that the chaperone system and the ubiquitin-proteasome system are closely coordinated to cope with the proteotoxic stress. Proteasomal function is inhibited by mutant SOD1 [19,36] and the expression of HSP70i has peaked out at the end stage of the disease even in the case of SOD1^{G93A}-L (Additional file 1: Figure S1). These data suggest that accumulation of proteotoxic species caused by proteasomal dysfunction could readily excess the capacity of the chaperone system. Therefore, coordinated activation of the chaperone system and protein degradation systems that include the ubiquitin-proteasome system and the autophagy system is critical to cope with the proteotoxicity of mutant SOD1 or other causative proteins of neurodegenerative diseases.

Conclusion

The genetic supplementation of SIRT1 can ameliorate a mutant SOD1-linked ALS mouse model partly through the positive regulation of the HSF1/HSP70i chaperone system. Future studies shall include identifying other downstream effectors and testing potential benefits of pharmacological enhancement of the deacetylation activity of SIRT1 after the onset of the symptom.

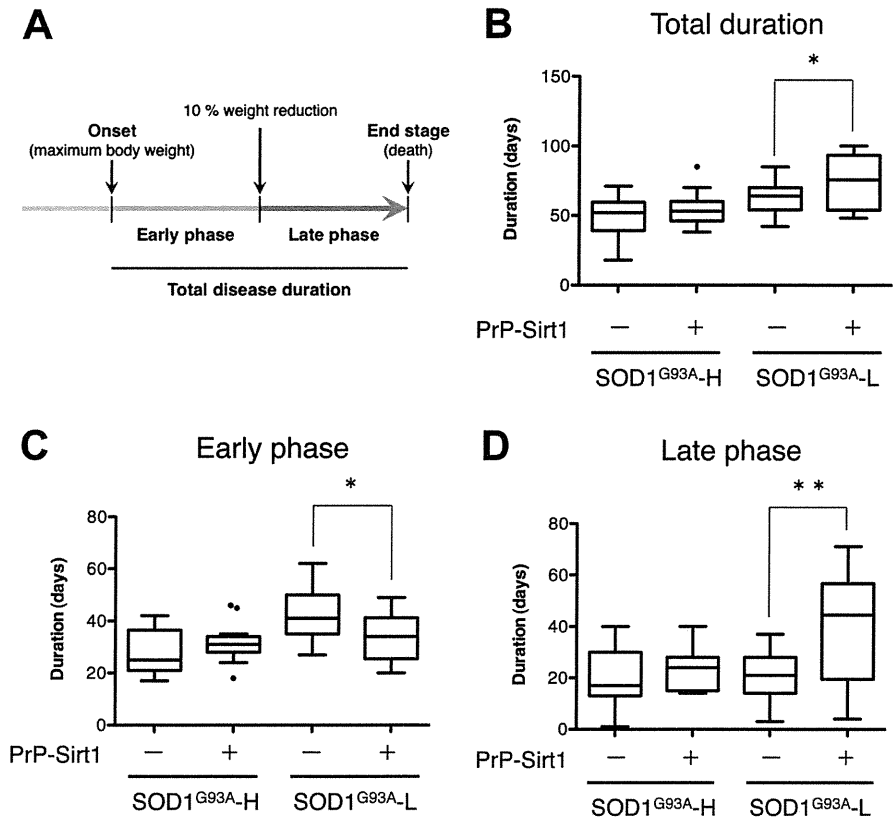

Figure 4 Effects of SIRT1 overexpression on the disease duration of non-transgenic, and high and low copy SOD1^{G93A} transgenic mice. **(A)** Definition of the early and late phases of the disease. **(B-D)** Comparison of the total **(B)**, early **(C)**, and late **(D)** phases of the disease duration. SIRT1 overexpression extended the total disease duration in the SOD1^{G93A}-L mice by extending the late phase. The data were analyzed by one-way ANOVA following post-hoc t-tests. *, $p < 0.05$; **, $p < 0.01$.

Materials and Methods

Generation of SIRT1 transgenic mice and crossbreeding with mutant SOD1 mice

To generate a line of transgenic mice that chronically overexpress SIRT1 in the central nervous system, we constructed a transcription unit by inserting the coding region of the mouse *Sirt1* cDNA into the MoPrP (mouse prion gene promoter)-polyA cassette (Figure 1A) [37]. We injected linearized MoPrP-*Sirt1* transcription unit with a genetic marker (mouse αA-crystallin promoter-driven enhanced green fluorescent protein (EGFP)) into C57BL/6 J mouse oocytes and obtained a founder that transmitted the transgene in Mendelian manner. The genotyping was done by polymerase chain reaction for an artificial sequence near the MoPrP-*Sirt1* junction. The transgenic line is to be deposited to RIKEN Bioresource Center. Sirt1 transgenic and non-transgenic control mice for behavioral analyses were bred as littermates. Transgenic mouse lines expressing human SOD1 gene with ALS-linked mutations, SOD1^{G93A}-H [B6.Cg-Tg(SOD1*G93A)1Gur/J] or loxSOD1^{G37R} [B6.Cg-Tg(SOD1-G37R) 1Dwc/J] were previously described [17,18]. SOD1^{G93A}-L was generated by a spontaneous drop of the copy number of the SOD1^{G93A}-H line, and has been maintained in our laboratory for several generations.

Animals and experimental design

All animal procedures were conducted in accordance with the guidelines of the Animal Use and Care Committees of Kyoto University, National Institute for Physiological Science, Nagoya University, and RIKEN. All comparisons were made between littermates to minimize confounding effects of different genetic background and environment. All behavioral tests were conducted at 5–9 months of age as described previously [38,39]. Mice were group housed (4 mice per cage) in a specific pathogen-free room kept at 23 ± 2°C with a 12 h light/dark cycle (lights on at 7 a.m.) with access to food and water. For survival experiments, SOD1^{G93A} mice were always compared with their littermates with PrP-Sirt1 gene. Times of disease onset, early phase, and end stage were determined respectively as the time when mice had started losing the maximum body weight, when denervation-induced muscle atrophy had produced a 10% loss of maximal weight, and when

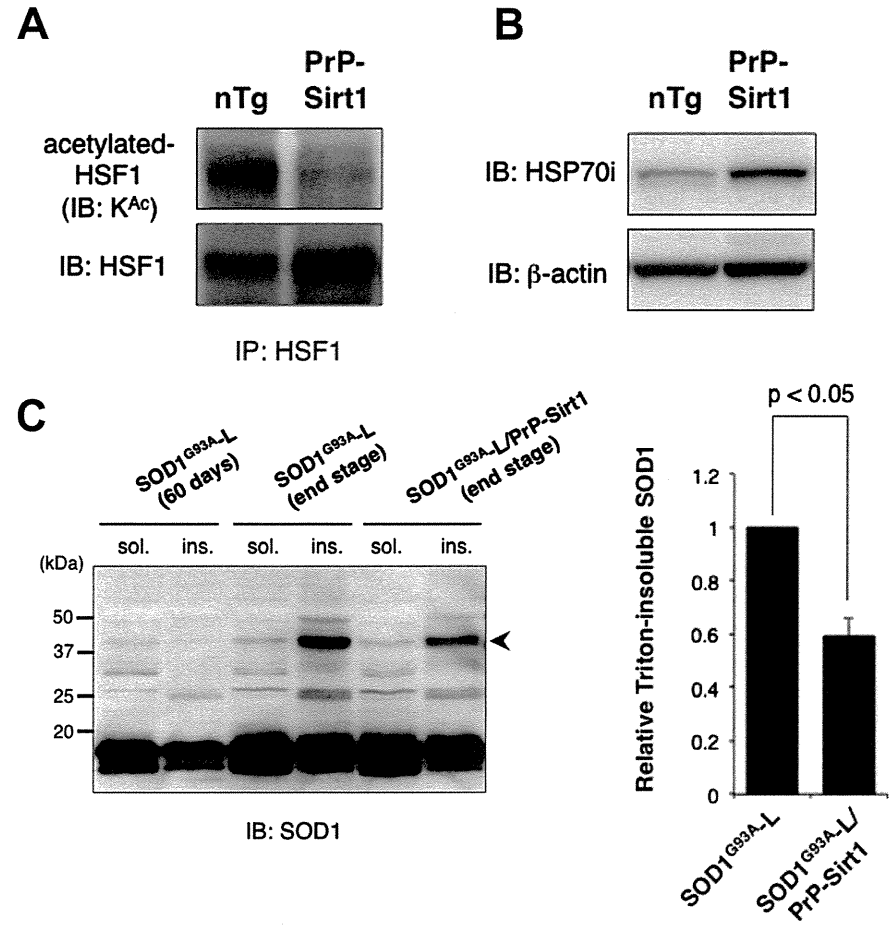

Figure 5 Effects of SIRT1 overexpression on the induction of HSP70i in the spinal cord of SOD1^{G93A}-L/PrP-Sirt1 transgenic mice. **(A)** HSF1 was significantly deacetylated in 5-month-old PrP-Sirt1 mouse spinal cord. Acetylated HSF1 was detected with anti-acetylated lysine antibody after the immunoprecipitation with anti-HSF1 antibody. **(B)** HSP70i was significantly induced in the PrP-Sirt1 mouse spinal cord. **(C)** Sirt1 overexpression reduced the insoluble SOD1 species in the end-stage SOD1^{G93A} mouse spinal cord. Triton X-100 insoluble and SDS-resistant SOD1^{G93A} dimer (arrowhead, ~40 kDa) was detected by immunoblotting (left panel). The relative densitometric values were shown as mean ± SEM (right panel). SIRT1 overexpression significantly suppressed aggregation and insolubilization of SOD1^{G93A}. Each lane in **A**, **C**, and **D** contained 15 μg of total protein and the similar results were obtained from three independent experiments.

animals in lateral position failed in righting within 20 seconds, an endpoint commonly used for mutant SOD1 expressing mice which is compliant with the requirements of the Animal Use and Care Committee. Disease progression was defined by the duration between the onset and disease end-stage. Statistical analysis of survival time and disease duration was performed with a log-rank test and one-way ANOVA following post-hoc t-tests, respectively. Analyses were carried out by using GraphPad Prism (GraphPad Software, La Jolla, CA).

Genotyping of mice

Mice harboring *PrP-Sirt1* transgene were identified by PCR using following primers; 5′-CAAGAGGTTGT TAATGAAGC-3′ and 5′-TTTCCTGTTGCCTTCAAT CAGCTATCG-3′.

Mice harboring *SOD1*^{G93A} or *SOD1*^{G37R} transgene were identified by PCR using following primers; the mouse *SOD1* gene fragment (850 bp) was amplified by mSOD-A primer: 5′-GTTACATATAGGGGTTTACTTCATAATCTG-3′ and h/mSOD-C primer: 5′-CAGCAGTCACATTGCCCARG TCTCCAACATG-3′, and human SOD1 gene fragment (750 bp) was amplified by hSOD-B primer: 5′-CCAA GATGCTTAACTCTTGTAATCAATGGC-3′ and h/ mSOD-C primer.

Antibodies

We used the following commercially available antibodies: anti-SIRT1 from EMD Millipore Corp. (Billerica, MA, USA), anti-β-actin from Sigma-Aldrich Co. LLC. (St. Louis, MO, USA), anti-acetylated lysine from Cell Signaling Technology Inc. (Danvers, MA, USA), anti-HSF1, anti-HSP70i